CellPress

Neuron
NeuroResource

Transgenic Mice for Intersectional Targeting of Neural Sensors and Effectors with High Specificity and Performance

Linda Madisen,[1] Aleena R. Garner,[1] Daisuke Shimaoka,[2] Amy S. Chuong,[3] Nathan C. Klapoetke,[3] Lu Li,[1] Alexander van der Bourg,[4] Yusuke Niino,[5] Ladan Egolf,[4] Claudio Monetti,[6] Hong Gu,[1] Maya Mills,[1] Adrian Cheng,[1] Bosiljka Tasic,[1] Thuc Nghi Nguyen,[1] Susan M. Sunkin,[1] Andrea Benucci,[2,5] Andras Nagy,[6] Atsushi Miyawaki,[5] Fritjof Helmchen,[4] Ruth M. Empson,[7] Thomas Knöpfel,[8] Edward S. Boyden,[3] R. Clay Reid,[1] Matteo Carandini,[2] and Hongkui Zeng[1,*]

[1]Allen Institute for Brain Science, 551 N 34th Street, Seattle, WA 98103, USA
[2]UCL Institute of Ophthalmology, University College London, 11-43 Bath Street, London, EC1V 9EL, UK
[3]MIT Media Lab and McGovern Institute, Massachusetts Institute of Technology, 20 Ames Street, Cambridge, MA 02139, USA
[4]Brain Research Institute, University of Zurich, Winterthurerstrasse 190, CH-8057 Zurich, Switzerland
[5]Brain Science Institute, RIKEN, 2-1 Hirosawa, Wako-city, Saitama 351-0198, Japan
[6]Lunenfeld-Tanenbaum Research Institute, Mount Sinai Hospital, 600 University Avenue, Toronto, ON M5G 1X5, Canada
[7]Department of Physiology, Brain Health Research Centre, University of Otago, PO Box 913, Dunedin 9054, New Zealand
[8]The Division of Brain Sciences, Department of Medicine, Imperial College London, 160 DuCane Road, London, W12 0NN, UK
*Correspondence: hongkuiz@alleninstitute.org
http://dx.doi.org/10.1016/j.neuron.2015.02.022

SUMMARY

An increasingly powerful approach for studying brain circuits relies on targeting genetically encoded sensors and effectors to specific cell types. However, current approaches for this are still limited in functionality and specificity. Here we utilize several intersectional strategies to generate multiple transgenic mouse lines expressing high levels of novel genetic tools with high specificity. We developed driver and double reporter mouse lines and viral vectors using the Cre/Flp and Cre/Dre double recombinase systems and established a new, retargetable genomic locus, TIGRE, which allowed the generation of a large set of Cre/tTA-dependent reporter lines expressing fluorescent proteins, genetically encoded calcium, voltage, or glutamate indicators, and optogenetic effectors, all at substantially higher levels than before. High functionality was shown in example mouse lines for GCaMP6, YCX2.60, VSFP Butterfly 1.2, and Jaws. These novel transgenic lines greatly expand the ability to monitor and manipulate neuronal activities with increased specificity.

INTRODUCTION

The brain comprises a large number of neuronal and non-neuronal cell types, whose connections and interactions are fundamental to its function. To observe and manipulate their activities selectively, the best available approach is genetic targeting of protein-based sensors and effectors to specific cell types (Huang and Zeng, 2013). In mice, the Cre/lox recombination system is the most widely used approach to access specific cell types, utilizing gene promoters or loci with specific expression patterns (Gerfen et al., 2013; Gong et al., 2007; Madisen et al., 2010; Taniguchi et al., 2011). However, cell populations defined by Cre driver lines are often heterogeneous, encompassing multiple brain regions and/or multiple cell types (Harris et al., 2014). Fundamentally, cell types are rarely defined by single genes, but rather by intersectional expression of multiple genes. Thus, it is imperative to develop intersectional genetic targeting approaches, combining regulatory elements from two or more genes to increase specificity of transgene expression. Important efforts have been made to develop transgenic intersectional approaches, most successfully with the combination of Cre and Flp site-specific recombinases (SSRs) (Dymecki and Kim, 2007; Dymecki et al., 2010; Kranz et al., 2010; Ray et al., 2011; Robertson et al., 2013). However, thus far, intersectional approaches have not been widely used in functional studies, due to the limited number of validated transgenic tools available.

The ongoing development of increasingly effective sensors and effectors offers extraordinary opportunities for studies of neuronal interactions and functions (Fenno et al., 2011; Huang and Zeng, 2013; Knöpfel, 2012). One issue with the practical utility of these tools is that they require high-level expression in cell populations of interest. Such high levels of expression can be obtained with techniques that result in high transgene copy numbers in individual cells, such as in utero electroporation and adeno-associated virus (AAV) infection. However, these approaches have limitations, including invasive surgical delivery, incomplete coverage of the desired cell population, variable levels of expression in different cells, and, in the case of viruses, potential cytotoxicity associated with long-term viral infection and/or uncontrolled gene expression.

Transgenic mouse lines that express high and heritable patterns of genetic tools in specific cell populations provide an alternative that can overcome at least some of these limitations (Zeng

and Madisen, 2012; Zhao et al., 2011). We previously establish a standardized Cre-reporter system in which transgene expression was driven by a strong, ubiquitous CAG promoter targeted to the Rosa26 locus (Madisen et al., 2010; Muzumdar et al., 2007), expressing fluorescent proteins, calcium sensor GCaMP3, and optogenetic activator ChR2(H134R) and silencers Arch and eNpHR3.0 (Madisen et al., 2010, 2012; Zariwala et al., 2012). Although proved useful in many applications (Ackman et al., 2012; Haddad et al., 2013; Issa et al., 2014; Jackman et al., 2014; Kheirbek et al., 2013; Lee et al., 2014; Nguyen-Vu et al., 2013; Pi et al., 2013), we and others have also identified limitations in the sensitivity or functionality of these reporters in other situations.

Currently the only transgenic mouse approach demonstrated to reliably achieve AAV-like high-level expression is the use of the Thy1.2 promoter in randomly integrated transgenes (Arenkiel et al., 2007; Dana et al., 2014; Feng et al., 2000; Zhao et al., 2008), presumably with multiple copies at the insertion site. Although powerful in driving tool gene expression, this approach also has drawbacks. Expression of transgenes driven by the Thy1.2 promoter is strongly position dependent, necessitating a screen of multiple founder lines to find potentially useful ones. Furthermore, adding Cre-dependent control, e.g., a floxed-stop cassette, to a multi-copy transgene is problematic because Cre could then induce recombination both within and between the different copies, resulting in reduced transgene copy numbers and variability of transgene expression among different cells.

We therefore undertook a systematic evaluation of multiple approaches aiming at more specific and more robust transgene expression. To complement existing Cre driver lines, we focused on the intersection of Cre with another recombinase or with a transcriptional activator. In addition, we built and validated a new docking site in a permissive genomic locus, the TIGRE locus (Zeng et al., 2008), which supports repeated targeting. By introducing a tTA-based transcriptional amplification approach to the TIGRE locus, all reporter lines doubly regulated by Cre and tTA drove robust expression of sensors and effectors at levels substantially higher than those in comparable Rosa-CAG-based reporters. Functional characterization of lines carrying representative optical tools under Cre and tTA control demonstrates their enhanced efficiency for studies of neuronal activity, both in vitro and in vivo.

RESULTS

In our effort to improve upon current strategies for cell-type-specific transgene expression, we explored three strategies for intersectional control: (1) reporter expression that depends on two independent SSRs from the ubiquitous Rosa26 locus, (2) Cre-dependent reporter expression from an endogenous locus targeted because of its cell-type-specific expression pattern, (3) reporter expression dependent on Cre and the transcriptional transactivator tTA from another ubiquitous genomic locus, TIGRE. Since the third strategy resulted in the most strongly enhanced transgene expression, we created a series of TIGRE reporter lines that show high-level expression of novel calcium, voltage, and glutamate sensors and optogenetic effectors. The complete list of new intersectional transgenic mouse lines and AAVs introduced in this paper (17 reporter lines, 4 driver lines, and 10 AAVs) is shown in Table 1. All other previously published mouse lines used in this study are listed in Table S1.

Dual-Recombinase Intersectional Strategies for Transgene Regulation Increase Specificity

An intersectional approach that has proven useful in transgenic studies is to use both Cre and Flp, expressed from separate driver lines using distinct regulatory sequences, to turn on a doubly controlled reporter allele (Dymecki et al., 2010). To incorporate this into our Rosa-CAG reporter system (Madisen et al., 2010) and to test additional recombinases such as Dre (Anastassiadis et al., 2009; Sauer and McDermott, 2004), we generated Cre/Flp or Cre/Dre double-dependent reporters, the Ai65(RCFL-tdT) line that contains FRT-stop-FRT (FRT: Flp recognition site) and LoxP-stop-LoxP double cassettes in front of tdTomato, and the Ai66(RCRL-tdT) line containing Rox-stop-Rox (Rox: Dre recognition site) and LoxP-stop-LoxP double cassettes (Figure 1A). We also generated driver lines expressing these recombinases in the *Pvalb* gene locus, Pvalb-2A-Flpe (Buchholz et al., 1998), Pvalb-2A-Flpo (Raymond and Soriano, 2007), and Pvalb-2A-Dre, through recombinase-mediated cassette exchange (RMCE) into our originally targeted Pvalb-2A-Cre line (Figure S1A). To evaluate the recombination efficiency and specificity, we generated triple transgenic (Tg) mice whose genealogy included a pan-GABAergic Cre line Slc32a1-IR-Cre (*Slc32a1* is also known as *VGAT*, a GABA vesicular transporter; IR stands for IRES [internal ribosome entry site]), one of the Pvalb-SSR lines, and Ai65 or Ai66 reporter.

Cre and Flp (both Pvalb-2A-Flpe and Pvalb-2A-Flpo) efficiently restricted transgene expression to cell populations with overlapping patterns of driver expression. In the Slc32a1-IR-Cre;Pvalb-2A-Flpo;Ai65(RCFL-tdT) triple Tg mouse, tdTomato expression was observed in a subset of cells in multiple areas, consistent with *Slc32a1*+/*Pvalb*+ expression pattern (Figure 1B). Reporter expression depended strictly on the presence of both Cre and Flp drivers (Figure S2A). Importantly, these triple Tg mice showed higher selectivity in expression than double Tg, Pvalb-2A-Cre;Ai14 mice, where Ai14 is a Rosa-CAG-based tdTomato reporter line (Madisen et al., 2010). In those mice, but not in the triple Tg mice, we found expression in cortical layer 5 pyramidal neurons and other non-interneuron cells, presumably arising from low-level or transient expression of the *Pvalb* gene (Figures S2B and S2C). Thus, the intersectional approach depending on two drivers provides increased specificity for targeting *Pvalb*+ GABAergic neurons.

We also combined Cre and Dre to produce an effective intersectional approach in Slc32a1-IR-Cre;Pvalb-2A-Dre;Ai66 (RCRL-tdT) triple Tg mice (Figure S3A). Control mice lacking Cre showed no reporter expression, but occasional tdTomato-positive cells in Cre+/Dre-/Ai66+ mice were observed. To further evaluate the Cre/Dre intersection, we generated another Dre-driver line, Nr4a2-SA-IR-Dre (*Nr4a2* is also known as *Nurr1*, a nuclear receptor with expression in dopamine neurons and in claustrum), and crossed it with Emx1-IR-Cre and Ai66. The resulting triple Tg mice showed specific, dense expression in claustrum and endopiriform nucleus (Figure 1C), consistent with adult brain areas known to express both *Emx1* and *Nr4a2*.

Table 1. Newly Generated Transgenic Mouse Lines and AAVs

Name[a]	Knockin Locus	Promoter Used	Expression Control	Gene Expressed	Function	JAX Stock Number
Ai65(RCFL-tdT)	Rosa26	CAG	Cre and Flp dependent	tdTomato	Fluorescent labeling	021875
Ai66(RCRL-tdT)	Rosa26	CAG	Cre and Dre dependent	tdTomato	Fluorescent labeling	021876
Ai57(RCFL-Jaws)	Rosa26	CAG	Cre and Flp dependent	Jaws-GFP-ER2	Optogenetic silencer	(not deposited)
Ai72(RCL-VSFPB)	Rosa26	CAG	Cre dependent	VSFP-Butterfly 1.2	Voltage indicator	(not deposited)
Ai87(RCL-iGluSnFR)	Rosa26	CAG	Cre dependent	iGluSnFR	Glutamate indicator	(not deposited)
Ai95(RCL-GCaMP6f)	Rosa26	CAG	Cre dependent	GCaMP6f	Calcium indicator	024105
Ai96(RCL-GCaMP6s)	Rosa26	CAG	Cre dependent	GCaMP6s	Calcium indicator	024106
Ai62(TITL-tdT)	TIGRE	TRE	Cre and tTA dependent	tdTomato	Fluorescent labeling	022731
Ai82(TITL-GFP)	TIGRE	TRE	Cre and tTA dependent	EGFP	Fluorescent labeling	023532
Ai79(TITL-Jaws)	TIGRE	TRE	Cre and tTA dependent	Jaws-GFP-ER2	Optogenetic silencer	023529
Ai93(TITL-GCaMP6f)	TIGRE	TRE	Cre and tTA dependent	GCaMP6f	Calcium indicator	024103
Ai94(TITL-GCaMP6s)	TIGRE	TRE	Cre and tTA dependent	GCaMP6s	Calcium indicator	024104
Ai92(TITL-YCX2.60)	TIGRE	TRE	Cre and tTA dependent	YCX2.60	Calcium indicator	In process
Ai78(TITL-VSFPB)	TIGRE	TRE	Cre and tTA dependent	VSFP-Butterfly 1.2	Voltage indicator	023528
Ai85(TITL-iGluSnFR)	TIGRE	TRE	Cre and tTA dependent	iGluSnFR	Glutamate indicator	In process
Snap25-LSL-2A-GFP	Snap25	Snap25	Pan-neuronal promoter, Cre dependent	EGFP	Fluorescent labeling	021879
Snap25-2A-GCaMP6s	Snap25	Snap25	Pan-neuronal promoter	GCaMP6s	Calcium indicator	025111
Pvalb-2A-Flpe	Pvalb	Pvalb	Driver line	Enhanced Flp	Recombination	021191
Pvalb-2A-Flpo	Pvalb	Pvalb	Driver line	Mammalianized Flp	Recombination	022730
Pvalb-2A-Dre	Pvalb	Pvalb	Driver line	Mammalianized Dre	Recombination	021190
Nr4a2-SA-IR-Dre	Nr4a2	Nr4a2	Driver line	Mammalianized Dre	Recombination	(not deposited)
AAV pmSyn1-EBFP-Cre-bGHpA	–	Mouse Syn1	Driver	EBFP-Cre	Recombination	–
AAV phSyn1-Dre-bGHpA	–	Human Syn1	Driver	Mammalianized Dre	Recombination	–
AAV phSyn1-Flpo-bGHpA	–	Human Syn1	Driver	Mammalianized Flp	Recombination	–
AAV phSyn1-Flpe-bGHpA	–	Human Syn1	Driver	Enhanced Flp	Recombination	–
AAV phSyn1-FSF-FLEX-ChR2(H134R)-EYFP-WPRE-bGHpA	–	Human Syn1	Cre and Flp dependent	ChR2(H134R)-EYFP	Optogenetic activator	–
AAV phSyn1-RSR-FLEX-ChR2(H134R)-EYFP-WPRE-bGHpA	–	Human Syn1	Cre and Dre dependent	ChR2(H134R)-EYFP	Optogenetic activator	–
AAV pCAG-FSF-FLEX-EGFP-WPRE-bGHpA	–	CAG	Cre and Flp dependent	EGFP	Fluorescent labeling	–
AAV pCAG-FLEX2-tTA2-WPRE-bGHpA	–	CAG	Cre-dependent driver	tTA2	Transcriptional activation	–
AAV pTRE-FLEX-EGFP-WPRE-bGHpA	–	TRE	Cre and tTA dependent	EGFP	Fluorescent labeling	–
AAV pTRE-FSF-FLEX-EGFP-WPRE-bGHpA	–	TRE	Cre, Flp and tTA dependent	EGFP	Fluorescent labeling	–

[a]Acronyms: RCFL is Rosa26 – CAG promoter – FRT-STOP-FRT – LoxP-STOP-LoxP. RCRL is Rosa26 – CAG promoter – Rox-STOP-Rox – LoxP-STOP-LoxP. RCL is Rosa26 – CAG promoter – LoxP-STOP-LoxP. TITL is TIGRE – Insulators – TRE promoter – LoxP-STOP-LoxP. LSL is LoxP-STOP-LoxP. SA is Splice Acceptor. tdT is tdTomato. The 2A sequences used were F2A for Snap25-LSL-2A-GFP, and T2A for Snap25-2A-GCaMP6s, Pvalb-2A-Flpe, Pvalb-2A-Flpo, and Pvalb-2A-Dre.

Again, we observed no reporter expression in the absence of Cre but did detect sparse tdTomato-positive cells in Cre+/Dre-/Ai66+ mice (Figure S3B). This result suggests that while Dre specifically recombines Rox sites over Lox sites, Cre is slightly promiscuous toward Rox sites.

To complement our transgenic lines that incorporate dual recombinase control, we also generated a set of recombinant AAVs expressing Cre, Flpe, Flpo, and Dre drivers, as well as Cre/Flp and Cre/Dre doubly regulated reporters (Figures S4A–S4D). Consistent with previous reports (Fenno et al., 2014; Kranz

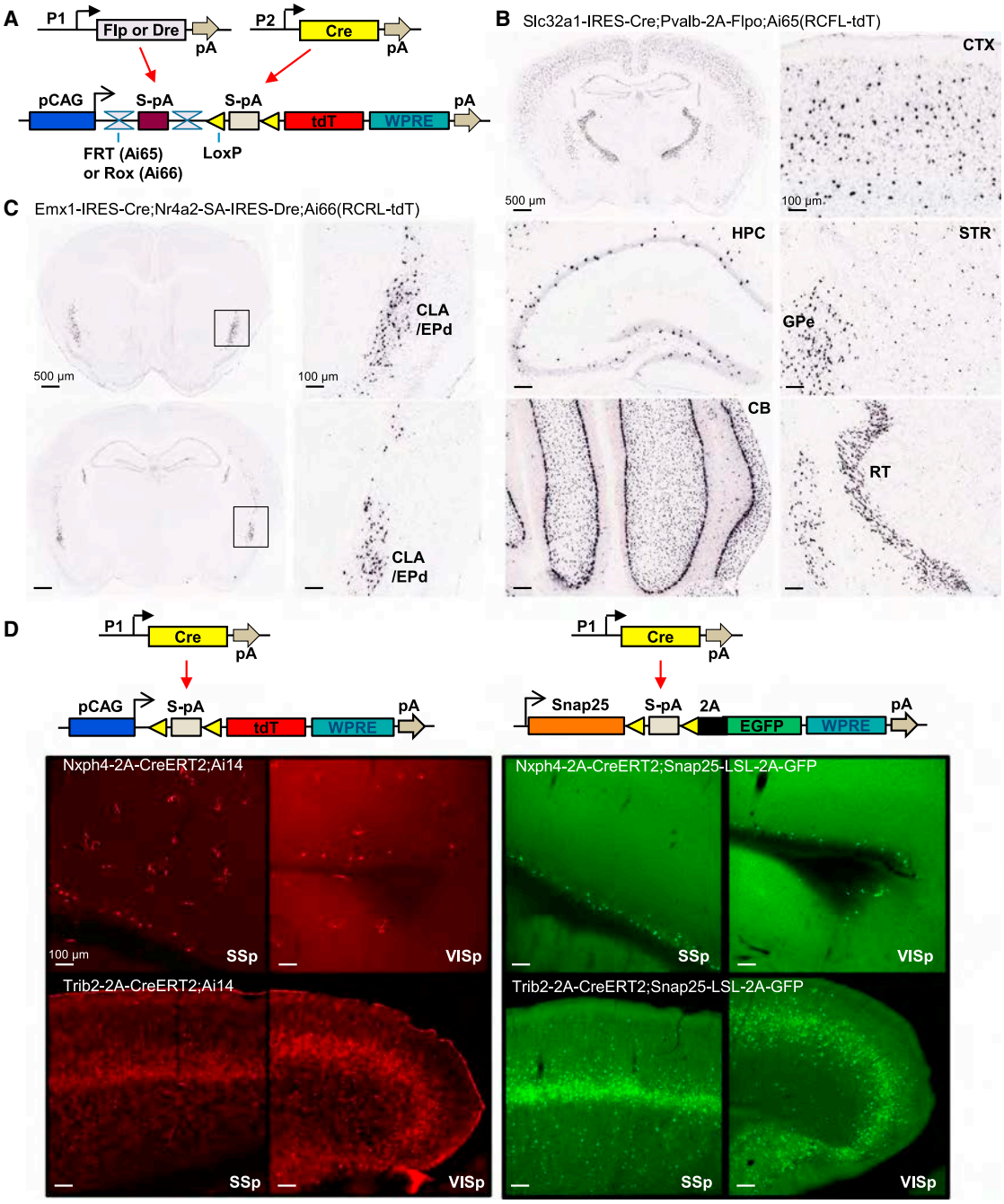

Figure 1. Intersectional Strategies Using Dual Recombinases or Cre Regulation of a Direct Neuronally Restricted Reporter

(A) Schematic diagram of intersectional control by either Cre/Flp or Cre/Dre recombinases, driven by different promoters (P1 or P2), on a doubly regulated reporter line: the Cre- and Flp-dependent Ai65(RCFL-tdT), or the Cre- and Dre-dependent Ai66(RCRL-tdT).

(B) ISH images of restricted tdTomato expression in *Slc32a1+/Pvalb+* GABAergic neurons in the Slc32a1-IR-Cre;Pvalb-2A-Flpo;Ai65(RCFL-tdT) mouse. CTX, cortex; HPC, hippocampus; STR, striatum; GPe, globus pallidus, external segment; CB, cerebellum; RT, reticular nucleus of the thalamus.

(C) ISH images of restricted tdTomato expression in *Emx1+/Nr4a2+* neurons in the claustrum (CLA) and endopiriform nucleus dorsal part (EPd) in the Emx1-IR-Cre;Nr4a2-SA-IR-Dre;Ai66(RCRL-tdT) mouse.

(D) Direct neuronally restricted reporter gene expression by targeting Cre-dependent reporter gene to the pan-neuronal *Snap25* gene locus. TdTomato expression in cortex in both neuronal and non-neuronal cells of Nxph4-2A-CreERT2;Ai14 and Trib2-2A-CreERT2;Ai14 mice (left) compared with neuronally specific EGFP expression in Nxph4-2A-CreERT2;Snap25-LSL-2A-GFP and Trib2-2A-CreERT2;Snap25-LSL-2A-GFP mice (right). SSp, primary somatosensory cortex; VISp, primary visual cortex. (See also Figures S1–S4.)

et al., 2010), AAV-Flpo- and AAV-Dre-induced recombination comparable to AAV-Cre, whereas the recombination efficiency of AAV-Flpe was significantly lower. Flp and Dre viruses exhibited high specificity for FRT and Rox sites, respectively, whereas AAV-Cre recombined Rox sites at low frequency, with recombination most prevalent at the injection site, indicating increased promiscuity with high levels of Cre.

Direct Neuronally Restricted Reporter Gene Expression

To determine whether a simple intersectional strategy could restrict Cre-induced reporter expression to a specific cell type, we took advantage of the *Snap25* gene. *Snap25* encodes a synaptosome-associated protein. It is pan-neuronal and is among the most highly transcribed genes in the brain based on microarray data analysis (data not shown). We generated a Snap25-LSL-2A-GFP knockin line, where a floxed-stop cassette and T2A-linked EGFP reporter gene is targeted to the stop codon of *Snap25* (Figure 1D). We then assessed fluorescent reporter expression in double Tg mice containing Cre drivers, Nxph4-2A-CreERT2 or Trib2-2A-CreERT2, crossed to either Ai14 or Snap25-LSL-2A-GFP reporters.

In both sets of animals crossed to Ai14, we found both neuronal and non-neuronal expression (Figure 1D, left). In Nxph4-2A-CreERT2;Ai14 (*Nxph4* is neurexophilin 4), we observed sparse cortical layer 6b expression but also significant expression in small, possibly glial cells. Likewise, in Trib2-2A-CreERT2;Ai14 (*Trib2* is tribbles homolog 2), we saw enriched expression in layer 5a cortical neurons but also strong and widespread fluorescence in vasculature. When crossed to Snap25-LSL-2A-GFP; however, EGFP expression in both lines was restricted to neurons, thereby increasing uniformity in the labeled cell populations (Figure 1D, right). Snap25-LSL-2A-GFP also showed stronger GFP fluorescence than the Rosa-CAG based Ai3-EYFP reporter (Madisen et al., 2010) (data not shown).

The pan-neuronal expression strategy can also be employed to restrict the functionality of other genetic tools to facilitate more precise observation or manipulation of cell populations. To this end, we generated a Snap25-2A-GCaMP6s knockin line, which expresses a calcium indicator GCaMP6s (Chen et al., 2013) pan-neuronally and independently of any driver line (Table 1). This line can be used to monitor neuronal calcium activity throughout the brain (Michael Crair and H.Z., unpublished data), while being readily combined with Cre- or another driver-dependent, cell-type-specific genetic manipulation.

Cre/tTA-Dependent Reporters Targeted to the TIGRE Locus Are More Highly Expressed than Rosa-CAG Reporters

The tetracycline (Tet)-regulated expression system has been used in mice for inducible expression of genes from the TRE (tetracycline response element, also called tetO) promoter in response to tTA (Tet-Off) or rtTA (Tet-On) activation (Garner et al., 2012; Gossen and Bujard, 1992; Mayford et al., 1996; Reijmers et al., 2007; Urlinger et al., 2000). Previous work showed that TRE-driven genes targeted (via a retrovirus) to the mouse TIGRE locus, situated on chromosome 9 between the *AB124611* (HIDE1) and *Carm1* loci, could be expressed in most tissues in the presence of tTA (Zeng et al., 2008). However, targeting of TRE-driven transgenic cassette to the Rosa26 locus resulted in silencing or mosaicism of the transgene expression (Tasic et al., 2012). To determine whether tTA/TRE can drive high-level expression in a defined locus, we created an expression platform in the TIGRE locus by homologous recombination. To establish feasibility, we first generated a tdTomato reporter allele, whose expression depends on both activation of the TRE promoter and Cre recombinase activity (Figure 2A). To prevent undesirable interactions with nearby chromatin, we flanked the reporter allele with two copies of the chicken β-globin HS4 insulator element (Chung et al., 1997; Gaszner and Felsenfeld, 2006) on each side. We named this new reporter line Ai62(TITL-tdT), to represent the TIGRE-Insulators-TRE promoter-LSL-tdTomato components.

To compare Ai62 with Ai14, we generated a series of double and triple Tg mice containing tdTomato-, Cre-, and/or tTA-expressing alleles and evaluated native fluorescence in brain sections (Figure 2B). We used three different tTA lines with our TIGRE mice: Camk2a-tTA (Mayford et al., 1996), ROSA:LNL:tTA (Wang et al., 2008), and ROSA26-ZtTA (Li et al., 2010) (Table S1), to test whether their varying tTA expression levels would influence the amount of reporter produced. Camk2a-tTA is restricted to forebrain excitatory neurons and striatal medium spiny neurons. The other two tTA lines are both targeted to the Rosa26 locus and contain floxed-stop cassettes and are thus presumed to have Cre-dependent ubiquitous expression. For a common Cre line, we used Nr5a1-Cre, which drives specific expression in cortical layer 4 neurons.

We observed robust tdTomato fluorescence in cortical layer 4 cells in all types of mice (Figure 2B). However, the fluorescence levels are different: lowest in Nr5a1-Cre;Ai14, followed by Nr5a1-Cre;ROSA:LNL:tTA;Ai62(TITL-tdT), then by Nr5a1-Cre;ROSA26-ZtTA;Ai62(TITL-tdT), and finally by Nr5a1-Cre;Camk2a-tTA;Ai62(TITL-tdT). Fluorescence-activated cell sorting (FACS) analysis of individual neurons isolated from cortical tissue of age-matched mice confirmed this result and revealed that tdTomato fluorescence per cell in each of the Ai62 triple Tg mice was 2- to 4-fold higher than that in Ai14 reporter cells (Figure S5). We tested specificity of expression of the TIGRE reporter Ai62 by generating mice that lacked either Cre or tTA. In these mice, we did not detect any fluorescence except for very weak fluorescence detected with Camk2a-tTA only. These results indicate that the Ai62 TIGRE reporter is tightly regulated (Figure 2C). Interestingly, we found that inclusion of the chromatin insulators is essential for high-level reporter expression, as a TIGRE reporter allele that lacks these insulators is poorly expressed in similar triple Tg animals (Figure 2D). The above comparison indicates that the TIGRE-targeted reporter is advantageous over Rosa26-CAG reporter in more robust transgene expression and the potential for additional specificity mediated through restricted tTA expression.

The new TIGRE allele differs from the Rosa26 allele in three key aspects: genomic location, use of the TRE promoter instead of the CAG promoter, and the flanking insulators. To begin to define which of these features contribute to the higher level of transgene expression apparent in Ai62 mice, we compared the expression of a pCAG-LSL-EGFP cassette that was targeted either to the TIGRE locus (with insulators) or to the Rosa26 locus (without insulators) in mouse ES cells (Figure S6). Following

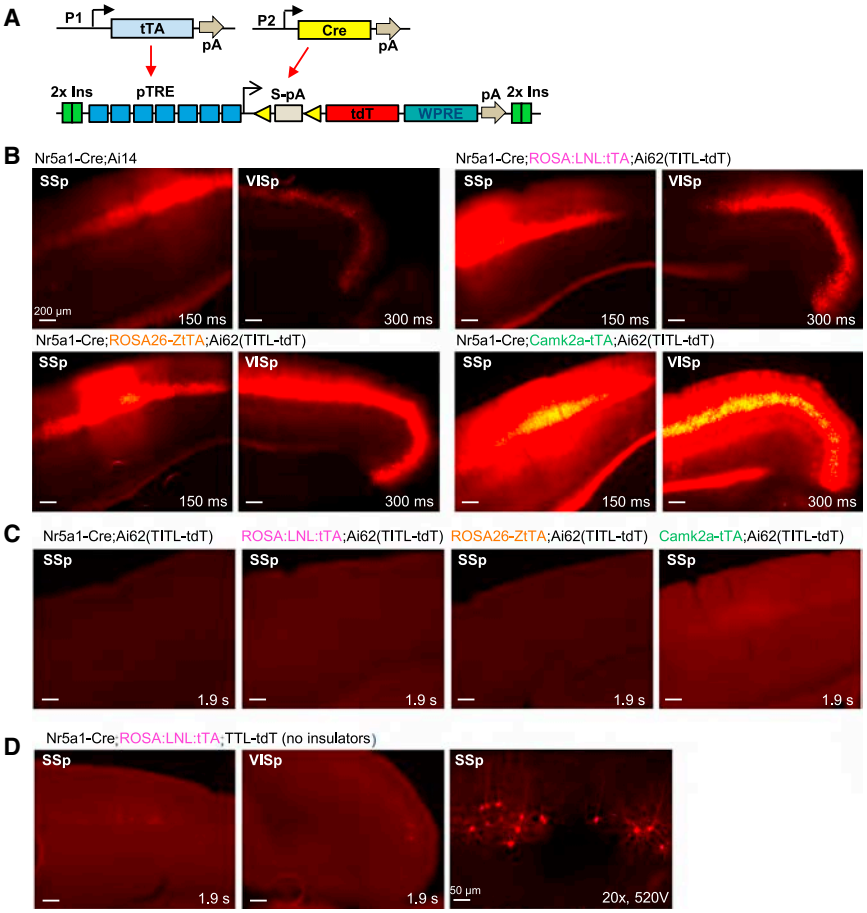

Figure 2. Cre- and tTA-Dependent Intersectional Strategy at the TIGRE Locus Produces Tightly Regulated and High-Level Expression

(A) Schematic diagram of intersectional control by Cre and tTA, driven by different promoters (P1 or P2), on a double reporter line based in the TIGRE locus, Ai62(TITL-tdT).

(B) Comparison of tdTomato fluorescence in four transgenic mouse lines carrying either Ai14 or Ai62 reporter alleles.

(C) No detectable tdTomato expression in the Cre+/tTA− control Nr5a1-Cre;Ai62(TITL-tdT) or in Cre−/tTA+ controls ROSA:LNL:tTA;Ai62(TITL-tdT) and ROSA26-ZtTA;Ai62(TITL-tdT). Very weak tdTomato fluorescence was seen in the barrel cortex and hippocampus of Camk2a-tTA;Ai62(TITL-tdT) control mice (Cre−/tTA+).

(D) Poor tdTomato expression in similar triple Tg mice with a TIGRE reporter (TTL-tdT) that lacks chromatin insulators (compare to B). Right: a higher-magnification confocal image of somatosensory cortex shows that the sparsely labeled cells are layer 4 neurons. For (B)–(D), exposure time for each epifluorescence image is shown for comparison. (See also Figures S4–S6.)

transient transfection of Cre into targeted clones to delete the stop cassettes, FACS analysis of two independent clones with each targeted locus showed comparable levels of EGFP fluorescence in all. Thus, we conclude that the difference in expression levels between Rosa26 and TIGRE mice is not simply due to the genomic location and the insulators; rather, it is more likely the result of the tTA/TRE-mediated transcriptional amplification (Iyer et al., 2001).

In addition to the transgenic reporter, we also generated AAV vectors to test the feasibility of Cre/tTA- and Cre/Flp/tTA-dependent regulation of virally encoded intersectional drivers and reporters. All reporters demonstrated the expected specificity of expression when paired with double or triple drivers, thereby further expanding the repertoire of viral tools that can be used for highly specific and versatile genetic control (Figures S4E–S4G).

New TIGRE Reporter Lines with Strong Expression of Sensors and Effectors

Based on the enhanced expression in Ai62, we proceeded to generate a series of TIGRE reporter lines carrying a variety of fluorescent sensors and optogenetic effectors (Table 1). This process was facilitated by our initial targeting strategy, which allows for subsequent rapid modification of the locus by RMCE (Figure S1B). In parallel, we generated Rosa26-based reporter lines for some of the same genes, including calcium indicators GCaMP6f and GCaMP6s (Chen et al., 2013), voltage indicator VSFP-Butterfly 1.2 (VSFPB) (Akemann et al., 2012), glutamate sensor iGluSnFR (Marvin et al., 2013), and red-light optogenetic inhibitor Jaws (Chuong et al., 2014), for further direct comparison between the Rosa-CAG and TIGRE-TRE expression systems.

We evaluated native fluorescence expression by confocal microscopy using identical imaging parameters for pairs of age-matched reporter mice crossed to the same Cre lines (Figure 3). Although the fluorescence level varies among different proteins, in all cases the same protein was more highly expressed from the TIGRE allele than from the Rosa26 allele. In addition, GCaMP6s expression in the TIGRE allele Ai94 was not only stronger than the Rosa-CAG allele Ai96 (Figure 3B), but also stronger than the Snap25-2A-GCaMP6s line, which, like Ai96, showed no basal level fluorescence (data not shown).

We observed strong expression of reporter transgenes when combining TIGRE alleles with a variety of Cre drivers and either Camk2a-tTA or ROSA26-ZtTA (Figure 4). The EGFP reporter line (Ai82) exhibited superior cytoplasmic labeling (Figure 4A) over previous Rosa-CAG reporter Ai3 (Madisen et al., 2010) and Snap25-LSL-2A-GFP (Figure 1D). We saw strong expression and proper localization to the plasma membrane in lines expressing membrane proteins VSFPB (Ai78; Figure 4B) and Jaws (Ai79; Figure 4F). The calcium indicator YCX2.60 (Ai92; Figure 4C) also displayed strong expression in both excitatory neurons and inhibitory interneurons. Likewise, cytoplasmic GCaMP6f (Ai93; Figure 4D) and GCaMP6s (Ai94; Figure 4E) were readily seen in cortical layer 4 and layer 2/3 excitatory neurons. In particular,

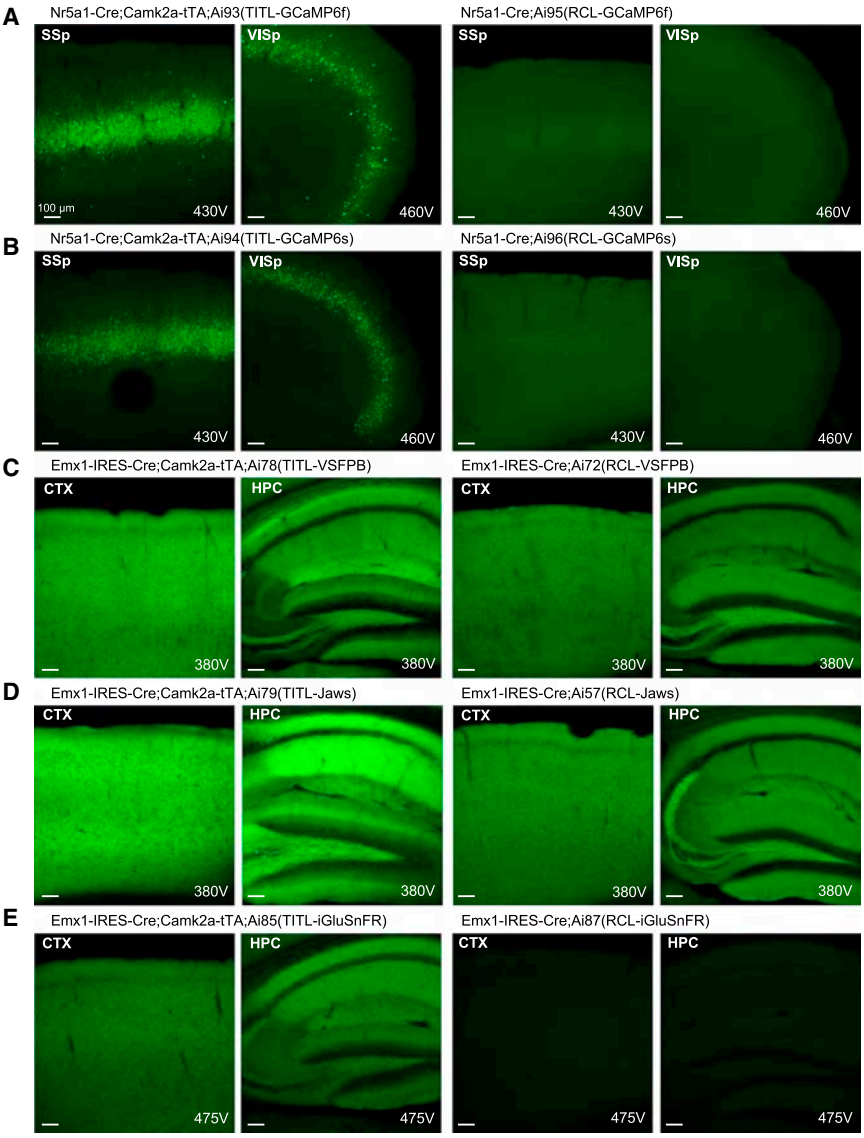

Figure 3. TIGRE Reporter Lines Have Higher-Level Transgene Expression than Rosa Reporter Lines in Multiple Direct Comparisons

Native fluorescence in each pair of lines was compared by confocal microscopy using identical imaging parameters. All images were taken under a 10× objective using 10% laser power, and the PMT gain (in voltage) is indicated on each image. Mouse names are shown above each set of images taken from the same mouse. Comparisons are shown for (A) GCaMP6f, (B) GCaMP6s, (C) VSFP-Butterfly 1.2, (D) Jaws-GFP-ER2, and (E) iGluSnFR. Ai57(RCL-Jaws) was created by crossing Ai57(RCFL-Jaws) with a Flp-deleter mouse, FLPeR, to delete the FSF cassette. (See also Figure S1.)

long-term, sustained expression of GCaMP6f in the Ai93 brain did not result in nuclear invasion (Figure 4G). This result contrasts the common observation associated with viral infection of GCaMP in which transgene expression continues to rise and leads to unhealthy cells whose nuclei become filled with fluorescence within weeks. Thus, these stable transgenic lines may allow longer-term repeated experimentation within the same animal. Nonetheless, animals expressing these engineered, exogenous proteins should still be used cautiously and monitored for possible unexpected adverse effects.

To further compare gene expression patterns in Rosa26 and TIGRE reporter lines, we evaluated mRNA expression in multiple lines by in situ hybridization (ISH) (Figure S7). All lines examined exhibited widespread and high-density expression in cortex when under the control of Emx1-IR-Cre alone (for Rosa26 lines) or in combination with Camk2a-tTA or ROSA26-ZtTA (for TIGRE lines) (Figure S7A). There was no significant difference in the numbers of expressing cells either between different lines or across ages. When regulated by some more specific Cre drivers, however, we found that although general expression patterns are similar between Rosa26 and TIGRE reporters, variations can occur depending on which tTA line is used for activation, with ROSA26-ZtTA tending to drive expression in fewer cells compared to Ai14, especially in subcortical regions (Figures S7B–S7D). These findings indicate that the interplay between Cre, tTA, and reporter alleles among different cells in different mouse lines may not always be predictable, thus reporter expression needs to be carefully assessed in new lines to ensure their applicability.

Imaging of Membrane Voltage in TIGRE-VSFPB Mice

To evaluate the TIGRE lines in functional measurements of neural activity, we tested transgenic line Ai78, which delivers a highly sensitive, genetically encoded voltage indicator, the voltage-sensitive fluroescent protein VSFP-Butterfly 1.2 (Akemann et al., 2012). This indicator reveals strong voltage signals in mouse sensory cortex, both under anesthesia and in wakefulness (Akemann et al., 2012; Carandini et al., 2015; Scott et al., 2014). It exhibits voltage-dependent Förster resonance energy transfer (FRET) between a pair of green and red fluorophores: mCitrine (donor) and mKate2 (acceptor). By imaging both fluorophores and taking the ratio of their fluorescence, one can obtain a good estimate of the underlying membrane voltage.

To study the functionality of the indicator in vitro, we imaged hippocampal slices from triple Tg mice Rasgrf2-2A-dCre; Camk2a-tTA;Ai78(TITL-VSFPB), which express the VSFP in the dentate granule cells of the hippocampus (Figure S8A). In these slices, a single shock to the perforant path evoked robust VSFP responses imaged over the dendritic field of dentate granule cells (Figure S8B). These responses could be observed both as increased acceptor signals and as decreased donor signals

(Akemann et al., 2012). We readily resolved VSFP transients above baseline noise in single sweeps (amplitude ~3–4× baseline noise, data not shown). Multiple stimulations (5×) at 100 Hz increased the VSFP response amplitude. The increase was sublinear, consistent with the temporal summation and well-known frequency-dependent depression of the synapses from medial perforant path to dentate granule cells (Petersen et al., 2013).

To address how well the indicator functions in vivo, we imaged a large portion of cerebral cortex on the left hemisphere (Figure 5A) of triple Tg mice Rasgrf2-2A-dCre;Camk2a-tTA;Ai78 (TITL-VSFPB), where layer 2/3 pyramidal cells express the VSFP (Figure 4B). The cortex exhibited approximately uniform expression (Figure 5B, apparent variations in brightness are due largely to inhomogeneous illumination; see also Figure S8C). This wide pattern of expression allowed us to image distinct sensory regions responsive to somatosensory, visual, or auditory stimuli in head-fixed, awake mice (Figure 5C). Showing visual stimuli in different horizontal and vertical positions (Figures 5D and 5F) allowed us to obtain maps of retinotopy covering multiple visual areas (Figures 5E and 5G), including V1, LM, and AL (Wang and Burkhalter, 2007). Presenting tones of different frequencies (Figure 5H) yielded maps of tonotopy in at least two auditory areas (A1 and AAF) (Hackett et al., 2011) (Figure 5I).

To measure signal/noise (S/N) ratios of voltage signals, we drove specific regions of sensory cortex with a periodic stimulus, making their activity oscillate. We then imaged this oscillating activity and divided the amplitude of the oscillation observed during stimulation with that observed in the absence of stimuli (Benucci et al., 2007). In response to optimally placed visual stimuli, visual cortex gave S/N ratios of 11.8 in the example mouse (Figure 5J) and similar values in five other mice (S/N = 12.1 ± 2.7 SEM). S/N ratios in these triple Tg mice were not statistically different ($p = 0.05$, Mann-Whitney test) from those seen in mice that expressed VSFP-Butterfly 1.2 following successful in utero electroporation (S/N = 5.6 ± 0.5, n = 3 mice) (Carandini et al., 2015).

Visual cortex responded faithfully to the visual stimuli, following the 4 Hz neural oscillations caused by reversals in visual contrast (Figure 5J). Visual cortex, however, also responded to the onset of air puffs, whether they were delivered toward the whiskers (Figure 5K) or away from them (Figure 5L), indicating that these responses were due to the sound of the air puffs, and specifically by the first puff in the train. Such cross-modal interactions have been described previously (Iurilli et al., 2012), and in our data may be compounded by occasional blinks. In contrast, somatosensory cortex responded only to the air puffs delivered to the whiskers (Figure 5N) and not to visual stimuli or to the sounds of the air puffs (Figures 5M and 5O). Finally, auditory cortex responded approximately equally to air puffs, whether they were delivered toward or away from the whiskers (Figures 5Q and 5R) and did not respond to visual stimuli (Figure 5P). These data indicate that VSFPB expressed by the Ai78 reporter is sufficiently sensitive to reliably and specifically record the membrane potential of neuronal populations, with fine temporal resolution.

In Vivo Recording of Calcium Signals in GCaMP6f and YCX2.60 Mice

GCaMP6 variants constitute the latest generation of genetically encoded calcium indicators (GECIs) (Chen et al., 2013) with fundamentally improved sensitivity and performance over previous generations, e.g., GCaMP3 and GCaMP5. We conducted in vivo two-photon imaging (Andermann et al., 2011; Bonin et al., 2011) through a cranial window over visual cortex in head-fixed, running GCaMP6 reporter mice and were able to simultaneously image hundreds of neurons relatively deep in the cortex (~300 μm below the pia surface, corresponding to visual cortical layer 4). Stimuli consisted of drifting sinusoidal gratings of five spatial frequencies (SFs), five temporal frequencies (TFs), and eight orientations (0° to 315° in 45° steps). In Scnn1a-Tg3-Cre;Camk2a-tTA;Ai93(TITL-GCaMP6f) triple Tg mice (Figures 6A–6C), GCaMP6f-labeled layer 4 neurons exhibited low baseline fluorescence in vivo (Figure 6A), while visual stimuli evoked responses with ΔF/F reaching 500% or higher (Figures 6A–6C). Visual responses selective for various orientations, SFs and TFs can be seen in different neurons (an example shown in Figure 6C).

Because of the low GCaMP6f fluorescence from the Rosa-CAG based Ai95 line (Figure 3A), we investigated whether Ai95 would still allow effective calcium imaging in comparison with Ai93. We measured neural activity from Ai95 and Ai93 under control of the pan-cortical driver Emx1-IR-Cre, i.e., in Emx1-IR-Cre;Ai95(RCL-GCaMP6f) (Figure 6D) and Emx1-IR-Cre;Camk2a-tTA;Ai93(TITL-GCaMP6f) (Figure 6E) mice. In both types of mice, robust fluorescent signal changes indicating neuronal activities were observed; however, signals were stronger in Ai93 than in Ai95 mice (compare bottom panels in Figures 6D and 6E). Additionally, the number of active neurons observable was significantly lower in Ai95 mice compared to Ai93 mice, especially deeper into the tissue (Figure 6F and Movies S1, S2, S3, and S4). Two-way ANOVA revealed a significant difference between genotypes, but not by depths and with no interaction (cells at 120-μm depth: Ai95 35 ± 5, Ai93 102 ± 18; cells at 300-μm depth: Ai95 18 ± 5, Ai93 129 ± 11, n = 3 mice each, $p = 4.6 \times 10^{-5}$ between genotypes). In addition, activity-related signal flashes can also be easily seen in processes corresponding to dendrites and axons in Ai93 mice (Movies S3 and S4). These results indicate that GCaMP6f expressed from both Ai95 and Ai93 mice yields signals responding to neuronal activities but that due to its higher expression level Ai93 may be more capable of detecting weaker neuronal activities.

Ratiometric imaging using FRET-based calcium indicators, such as yellow cameleon (YC) indicators (Horikawa et al., 2010; Nagai et al., 2004; Yamada et al., 2011), is another approach that has the advantage of reduced sensitivity to motion artifacts and essentially permits quantification of calcium concentration levels. YCX2.60, a new version of YC indicator with an expanded dynamic range (Figure 7A), also displayed strong expression in both excitatory neurons and inhibitory interneurons (Ai92, Figure 4C). We performed two-photon calcium imaging in layer 2/3 of somatosensory cortex in Rasgrf2-2A-dCre;Camk2a-tTA;Ai92(TITL-YCX2.60) mice and observed spontaneous and sensory-evoked neuronal activity with high sensitivity (Figures 7B–7D), confirming the functionality of the Ai92 mice.

Red Light-Mediated Optogenetic Inhibition in Jaws Mice

Jaws is the first red light drivable optogenetic inhibitor, engineered from *H. salinarum* (strain Shark) cruxhalorhodopin

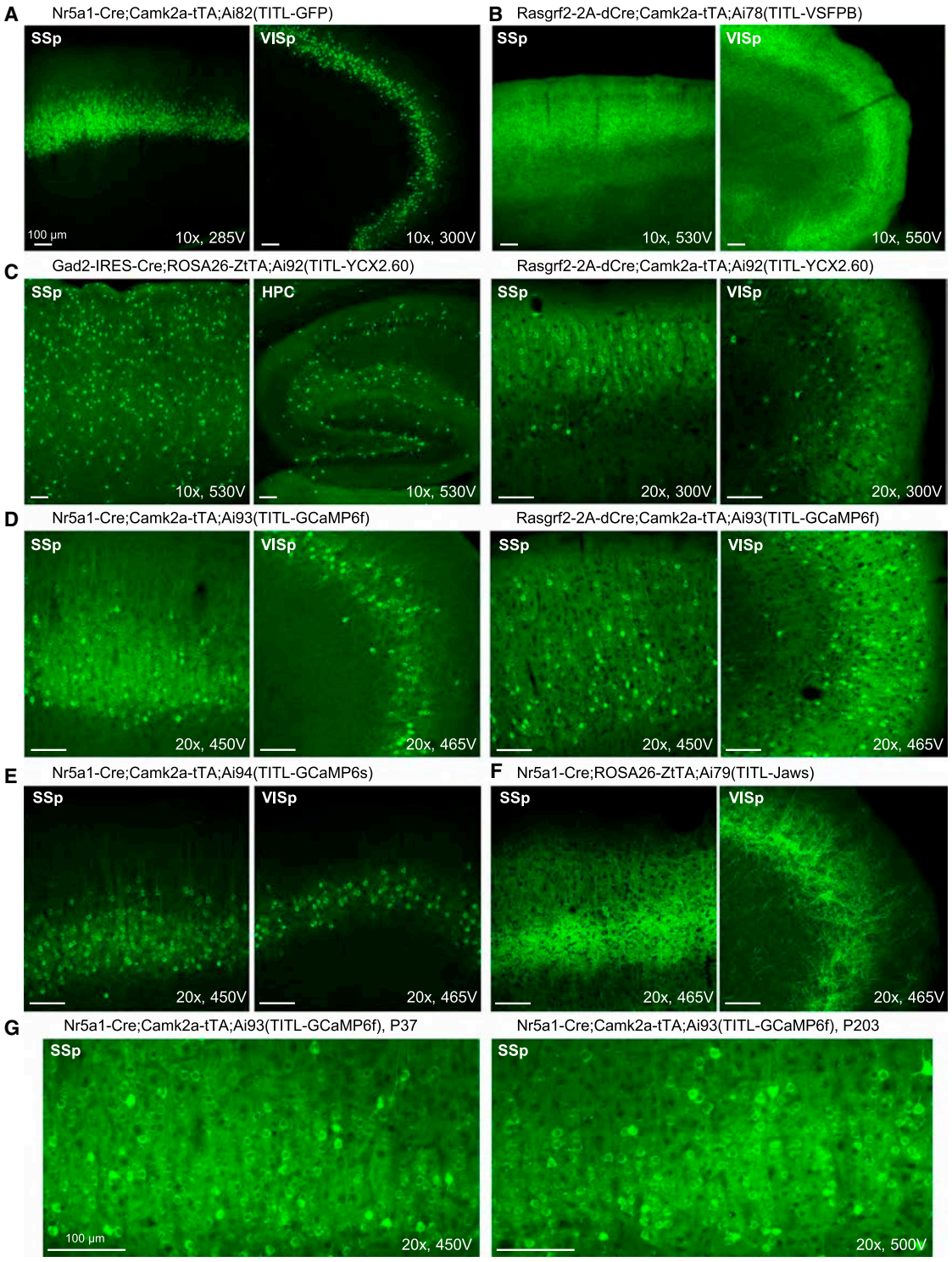

Figure 4. Strong Transgene Expression in all TIGRE-Based Reporter Lines, Driven by a Variety of Cre Lines Combined with Camk2a-tTA or ROSA26-ZtTA

Confocal images of native fluorescence are shown. All images were taken under a 10× or 20× objective using 10% laser power, and the PMT gain (in voltage) is indicated on each image for comparison.

(A) Very bright cytoplasmic GFP labeling of cortical layer 4 neurons in Nr5a1-Cre;Camk2a-tTA;Ai82(TITL-GFP) mouse.

(B) Bright membrane VSFP-Butterfly 1.2 labeling of cortical layer 2/3 neurons in Rasgrf2-2A-dCre;Camk2a-tTA;Ai78(TITL-VSFPB) mouse.

(legend continued on next page)

(Chuong et al., 2014). Compared with other photo-activated inhibitors such as eNpHR3.0, Arch, or ArchT, Jaws responds robustly to red light with high sensitivity, large photocurrent, and fast kinetics and thus enables better tissue penetrance and more effective optogenetic silencing of large volumes (Chuong et al., 2014). We compared the performance of a modified trafficking variant of Jaws, Jaws-GFP-ER2, expressed from the Rosa-CAG allele, i.e., Emx1-IR-Cre;Ai57(RCL-Jaws) mice (simplified as Ai57), and the TIGRE allele, i.e., Emx1-IR-Cre; Camk2a-tTA;Ai79(TITL-Jaws) mice (simplified as Ai79), via slice and in vivo electrophysiology, using virally expressed Jaws and Arch-expressing mice Ai35 as references (Chuong et al., 2014; Madisen et al., 2012) (Figure 8).

In brain slices, Jaws-expressing cells showed normal membrane properties (n = 13 cells in Ai57 mice, n = 17 in Ai79, n = 12 in Ai35, Figure S9A). Red light illumination (632 nm) induced strong hyperpolarizing currents in Jaws-expressing neurons in Ai79 mice and effectively blocked depolarization-induced spiking, whereas the light effect was small to moderate in Ai57 mice (Figures 8A–8C). Photocurrents were comparable between Ai79 and virally expressed Jaws at all irradiance levels tested but were significantly smaller in Ai57 cells (Figures 8D and 8E), consistent with the observation of stronger native fluorescence in Ai79 (Figure 3D). We also noticed that the Jaws-GFP-ER2 in Ai57 displayed lower protein fluorescence than the Arch-GFP-ER2 in the similar Rosa-CAG allele Ai35 (Figure S9C), possibly due to different protein properties (see Discussion below), but the low photocurrents generated were similar between the two (Figures 8D, 8E, and S9B).

Next, we assessed Jaws performance in vivo. We conducted extracellular recordings in the primary visual cortex of awake, head-fixed mice using glass pipettes and with a 200-μm optical fiber in place (Chuong et al., 2014). Due to the low photocurrents of Ai35 and Ai57 in slices, only Ai79 was tested in vivo. Ai79 showed strong red light (637 nm) induced suppression of spontaneous neuronal firing (Figures 8F and 8G; n = 23 units from 2 mice, n = 3 units showed no change). Light delivery through the fiber tip inhibited neuronal firing in a light intensity-dependent manner in these mice, comparable to the performance of virally expressed Jaws (Figure 8H).

DISCUSSION

We sought to develop transgenic strategies for intersectional control and to compare performance of these strategies under native conditions in the mouse brain. In addition to striving for high-level and highly specific expression of genetic tools, we aimed to generate standardized expression platforms, in a few defined genomic loci, that would allow rapid modification for future improvements and applications. Such efforts are more laborious and time consuming than other in vivo approaches, such as random transgenesis or viral infection, but they can provide more definitive evaluations and more consistent platforms for incorporating additional genetic tools and expansion into other cell types.

For example, we observed significant, heritable variation in protein expression among the various sensors and effectors (Figures 3 and 4), despite their having the same configuration within the TIGRE or Rosa26 alleles. We think this variation is most likely due to intrinsic protein properties, as they originate from diverse non-mammalian species. Protein engineering, such as codon optimization and addition of membrane-targeting tags (Gradinaru et al., 2010), is essential for optimizing expression in the mammalian brain. However, since many of the proteins we worked with had already undergone such engineering, the observed variation suggests that intrinsic differences still exist. Therefore expression in mice as a stably integrated transgene is unpredictable and always needs to be examined experimentally in vivo. Our data indicate that while the Rosa-CAG approach could work well for some proteins with exceptional expressibility and/or functionality, e.g., in Ai14-tdTomato, Ai32-ChR2(H134R) (Madisen et al., 2012) as well as Ai95-GCaMP6f mice, our new TIGRE approach, with its much enhanced gene expression capability via tTA-assisted transcriptional amplification, will allow a wider spectrum of genetic tools to achieve functional levels and/or to perform better in stable transgenic settings. This amplification proves to be significant even in comparison with expression from transgenes targeting one of the brain's most highly expressed endogenous genes, *Snap25*.

On the other hand, in our effort to create more cell-type-specific tTA driver lines, we found that several knockin tTA driver lines we made exhibit no or low-level tTA-induced reporter expression (Table S2). This may be because the Tet-regulatory system is prone to epigenetic silencing (Tasic et al., 2012; Zhu et al., 2007). Further investigation and optimization will be needed to expand the repertoire of tTA drivers to take full advantage of the potential of TIGRE-based reporters. Nevertheless, our work validates the currently available Camk2a-tTA and ROSA26-ZtTA lines as effective components of a TIGRE-based approach in driving robust transgene expression.

We have established the TIGRE locus as a new permissive docking site for insertion of exogenous promoters and transgenes. This is significant since TRE-driven transgene cassettes are often silenced when inserted into the mouse genome randomly or even targeted to specific loci such as Rosa26 (B.T., L.M., and H.Z., unpublished data; see also Li et al., 2010; Tasic et al., 2012; Zhu et al., 2007). Our expression studies also showed that both TRE and CAG promoters worked well in

(C) Very bright cytoplasmic YCX2.60 labeling of interneurons in Gad2-IR-Cre;ROSA26-ZtTA;Ai92(TITL-YCX2.60) mouse and of cortical layer 2/3 neurons in Rasgrf2-2A-dCre;Camk2a-tTA;Ai92(TITL-YCX2.60) mouse.

(D) Bright cytoplasmic GCaMP6f labeling of cortical layer 4 neurons in Nr5a1-Cre;Camk2a-tTA;Ai93(TITL-GCaMP6f) mouse and of cortical layer 2/3 neurons in Rasgrf2-2A-dCre;Camk2a-tTA;Ai93(TITL-GCaMP6f) mouse.

(E) Bright cytoplasmic GCaMP6s labeling of cortical layer 4 neurons in Nr5a1-Cre;Camk2a-tTA;Ai94(TITL-GCaMP6s) mouse.

(F) Bright membrane Jaws-GFP-ER2 labeling of cortical layer 4 neurons in Nr5a1-Cre;Rosa26-ZtTA;Ai79(TITL-Jaws) mouse.

(G) Comparison of young and old Ai93 mice shows no or little nuclear invasion of transgene proteins with time. The ages (postnatal days) at which the mice were sacrificed are shown. (See also Figure S7.)

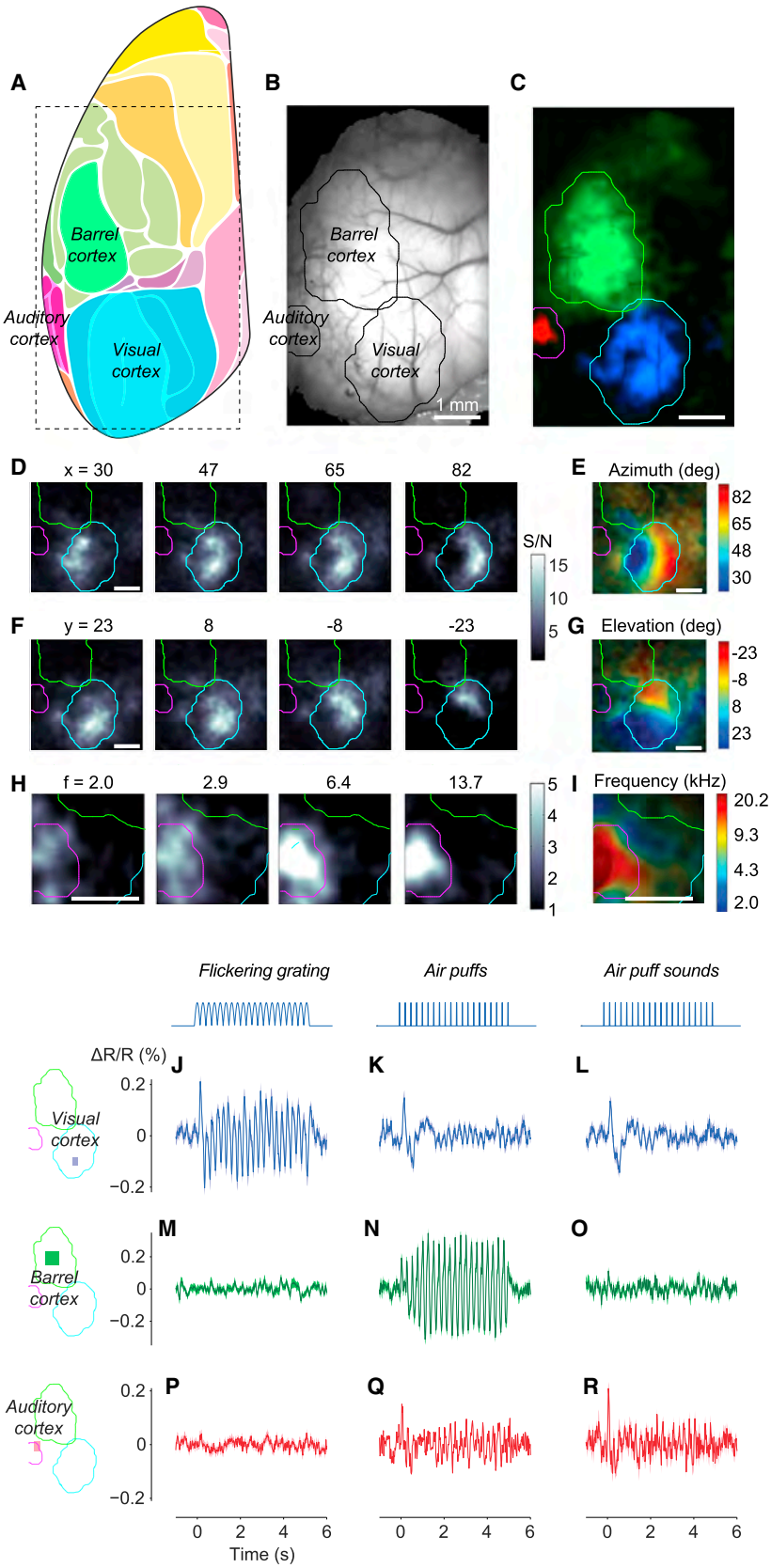

Figure 5. Wide-Field Imaging of Sensory Cortices of Ai78 Mice Expressing VSFP-Butterfly 1.2 in Cortical Layer 2/3 Excitatory Neurons

(A) Diagram showing mouse cortical regions observed from the top of the brain. Adopted and modified from Kirkcaldie (2012). The rectangle shows the approximate extent of our imaging area, which was angled at 30° relative to the vertical.

(B) Fluorescence of mCitrine imaged through the thinned skull.

(C) Maps of VSFP signals (acceptor-donor ratio) to auditory (red), somatosensory (green), and visual (blue) stimuli. Sensory regions are mapped as 4 Hz amplitude in response to 4 Hz train of tones, 4 Hz train of air puffs directed to whole whisker field, and 2 Hz flickering visual stimulus. Response amplitude was divided for each modality by amplitude measured in the absence of stimulation. The three maps came from experiments performed on different days, and the resulting maps were aligned based on the blood vessel pattern. Overlaid contour lines show the outlines of visual cortex, barrel cortex, and auditory cortex.

(D) Amplitude maps for 4 Hz responses to bars reversing in contrast at 2 Hz, presented at different horizontal positions (azimuths).

(E) The resulting maps of azimuth preference (retinotopy).

(F and G) Same as (D) and (E) for stimulus elevation (vertical position).

(H) Amplitude maps for 6 Hz responses to tones in 6 Hz trains, for different tone frequencies.

(I) The resulting maps of tone frequency preference (tonotopy).

(J–R) Unisensory and multisensory signals in visual cortex (J–L), barrel cortex (M–O), and auditory cortex (P–R). Stimuli were contrast-reversing visual gratings (J, M, and P), air puffs delivered to the whiskers (K, N, and Q), and (sham) air puffs delivered away from the whiskers to replicate the sound but not the somatosensory stimulation (L, O, and R). ΔR/R is calculated after normalization using data during the prestimulus period and high-pass filtering above 0.5 Hz. (See also Figure S8.)

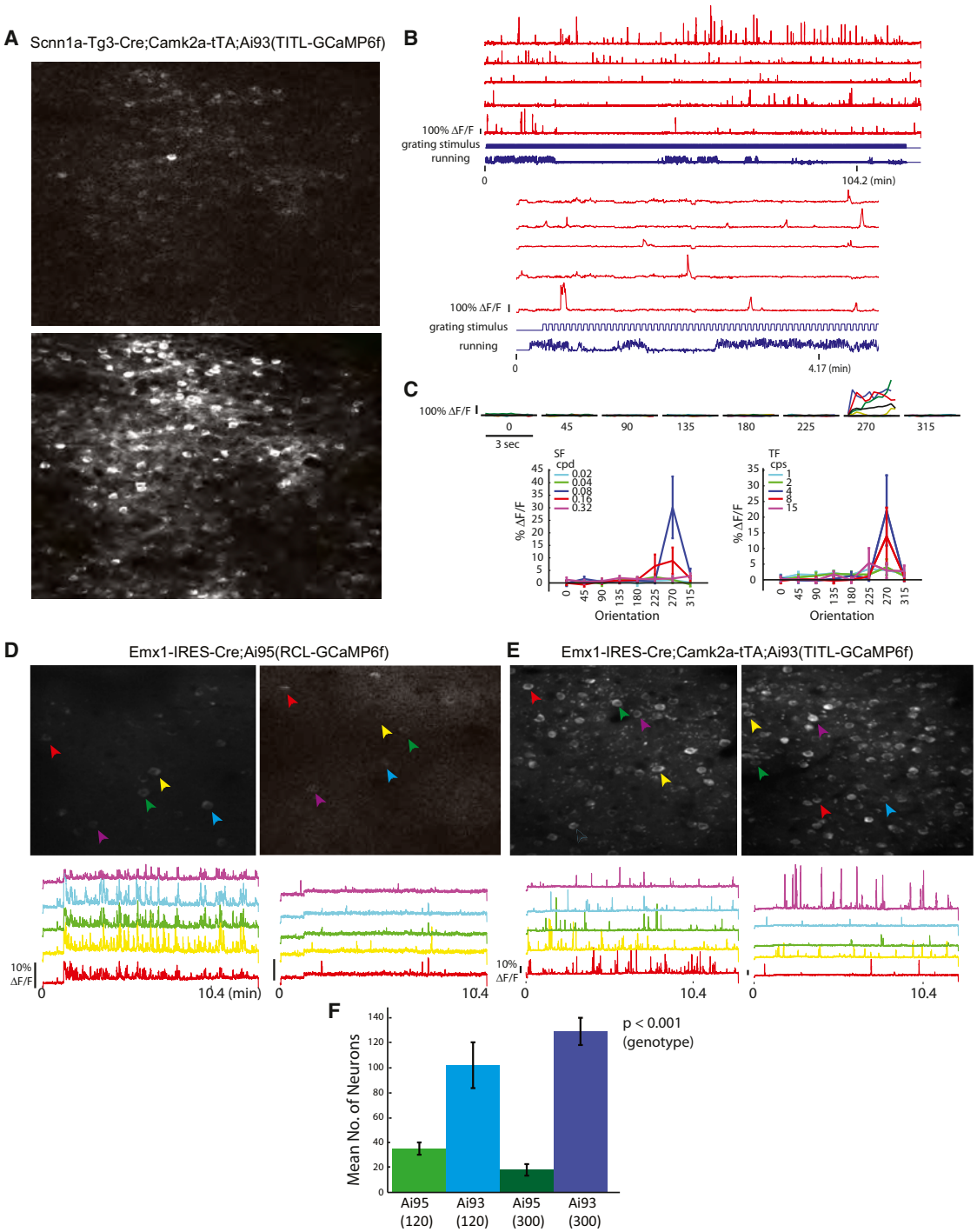

Figure 6. In Vivo Two-Photon Imaging of Calcium Signals in GCaMP6f Reporter Mice

(A–C) Calcium imaging in cortical layer 4 of Scnn1a-Tg3-Cre;Camk2a-tTA;Ai93(TITL-GCaMP6f) mice. (A) Images of baseline fluorescence with a single active cell (top) and Z projection (time series) of the same field of view showing all active cells (bottom). (B) Raw traces of five example neurons imaged during stimulus presentation. Top: the duration of the entire experiment. Bottom: the same five cells over a shorter timescale. The bottom cell trace is the cell analyzed for tuning properties shown in (C). (C) Visually evoked responses of an example cell. Top: peri-stimulus-time-histogram (PSTH) of the cell's response at each stimulus orientation at optimal SF and TF. Colored lines represent individual trials and the black line represents the mean. Bottom left: mean response at each SF (averaged over all TFs) as a function of orientation. Bottom right: mean response at each TF (averaged over all SFs) as a function of orientation.

(legend continued on next page)

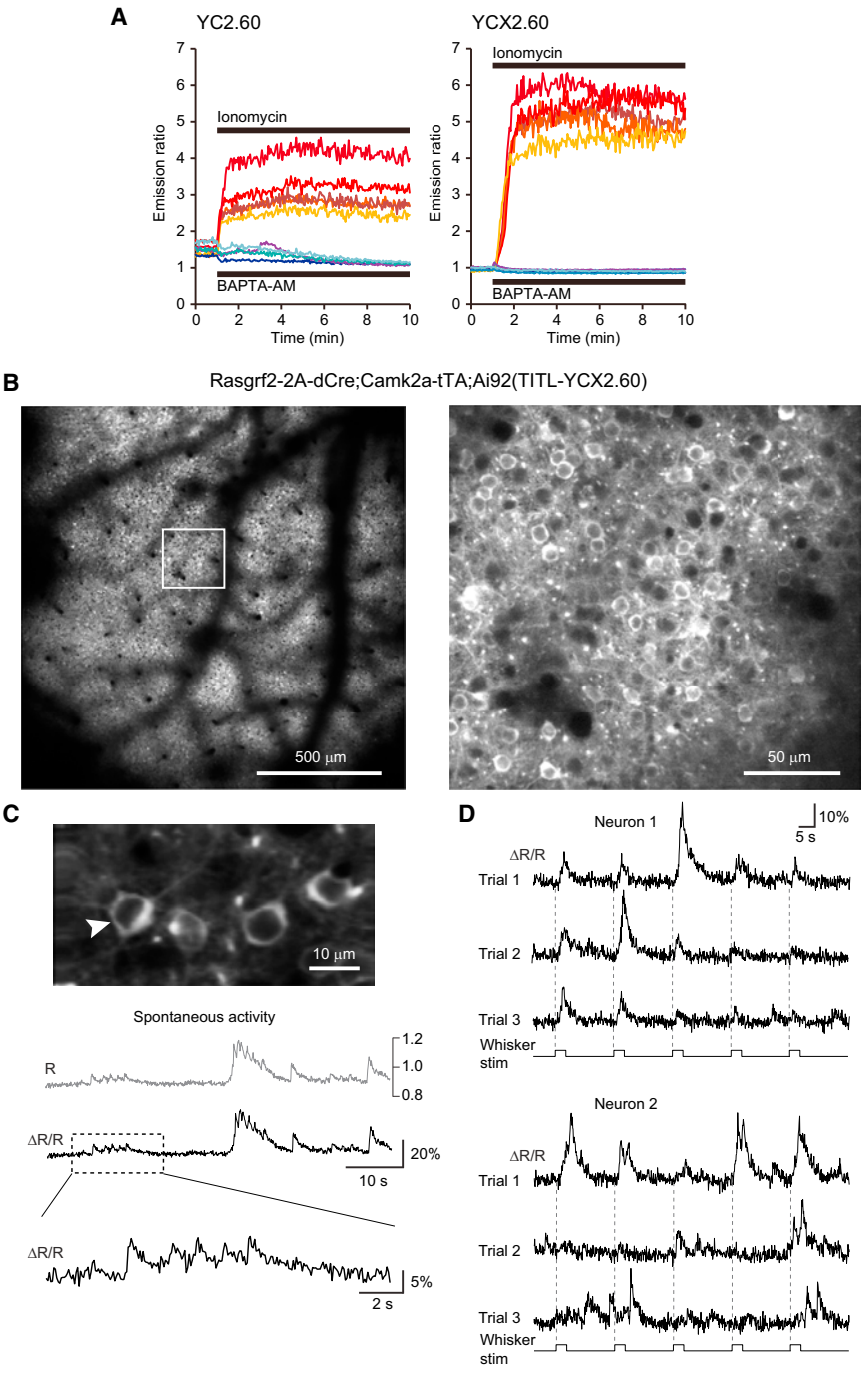

Figure 7. Calcium Measurements with Yellow Cameleon YCX2.60

(A) Responses in individual HeLa cells to ionomycin applied to saturate yellow cameleons (YCs) with calcium (n = 5) and to BAPTA-AM applied to deplete YCs of calcium (n = 4). The dynamic range of YCX2.60 is twice as large as that of YC2.60 (Rmax/Rmin = 6.20 versus 3.17). The apparent dissociation constants of YC2.60 and YCX2.60 for calcium were calculated as 80 nM and 220 nM, respectively (Y.N. and A.M., unpublished data).

(B–D) In vivo two-photon imaging of calcium signals in Rasgrf2-2A-dCre;Camk2a-tTA;Ai92(TITL-YCX2.60) mice. (B) Visualization of the uniform expression in layer 2/3 at 190-μm depth within the cranial window 1 week after TMP induction (field of view size 1.7 × 1.7 mm). Note the shadows from surface blood vessels. The image on the right is a magnified view of the boxed area in the left image, showing neuronal somata labeled with YCX2.60. (C) Representative 60 s example of spontaneous activity in the neuron marked with an arrow. Raw, unfiltered calcium transients are expressed once as YFP:CFP ratio R, which in principle can be calibrated in terms of absolute calcium concentration or as relative percentage change of the ratio R (ΔR/R). The expanded view of the trace segment in the box highlights fast calcium transients presumably evoked by few or single action potentials. (D) Evoked activity in two example neurons following whisker stimulation. The principal whisker was repeatedly stimulated at 10 Hz for 2 s (onsets indicated with dashed lines). YCX2.60 ΔR/R traces are shown for two example layer 2/3 neuron for three trials, each comprising five stimulation periods. Note responses at stimulus onset, during stimulation, and at stimulus offset as well as spontaneous activity in between. Large calcium transients probably correspond to bursts of action potentials whereas small-amplitude transients may reflect occurrence of only few or single action potentials.

TIGRE, suggesting that this locus can also serve as a docking site for insertion of other promoters and regulatory sequences. This could be particularly useful, for example, for the screening of enhancer elements or promoter variants. To facilitate repeated use of these expression platforms, we have built a cassette exchange mechanism into each, based on reconstitution of a split-hygromycin selectable marker (Figure S1). By doing so, the swapping of either alternative drivers in targeted lines or new genetic tools in the TIGRE allele becomes a rapid and straightforward process, thereby extending the utility of these systems.

(D–F) Comparison of Emx1-IR-Cre;Ai95(RCL-GCaMP6f) and Emx1-IR-Cre;Camk2a-tTA;Ai93(TITL-GCaMP6f) mice at two imaging depths, 120 μm and 300 μm below the pia, corresponding to cortical layers 2/3 and 4, respectively. (D) Z projection of two-photon acquisition frames 120 μm (left) and 300 μm (right) below the pia of Ai95 mice. Raw traces of neural activity during ~10 min of visual stimulus presentation for five representative cells are shown below each image panel. (E) Same as (D) for Ai93 mice. (F) Mean number of cells from which activity could be observed during a 10 min imaging period at 120 μm and 300 μm depths within a 250 × 150 μm imaging area. All values represent mean ± SEM (See also Movies S1, S2, S3, and S4).

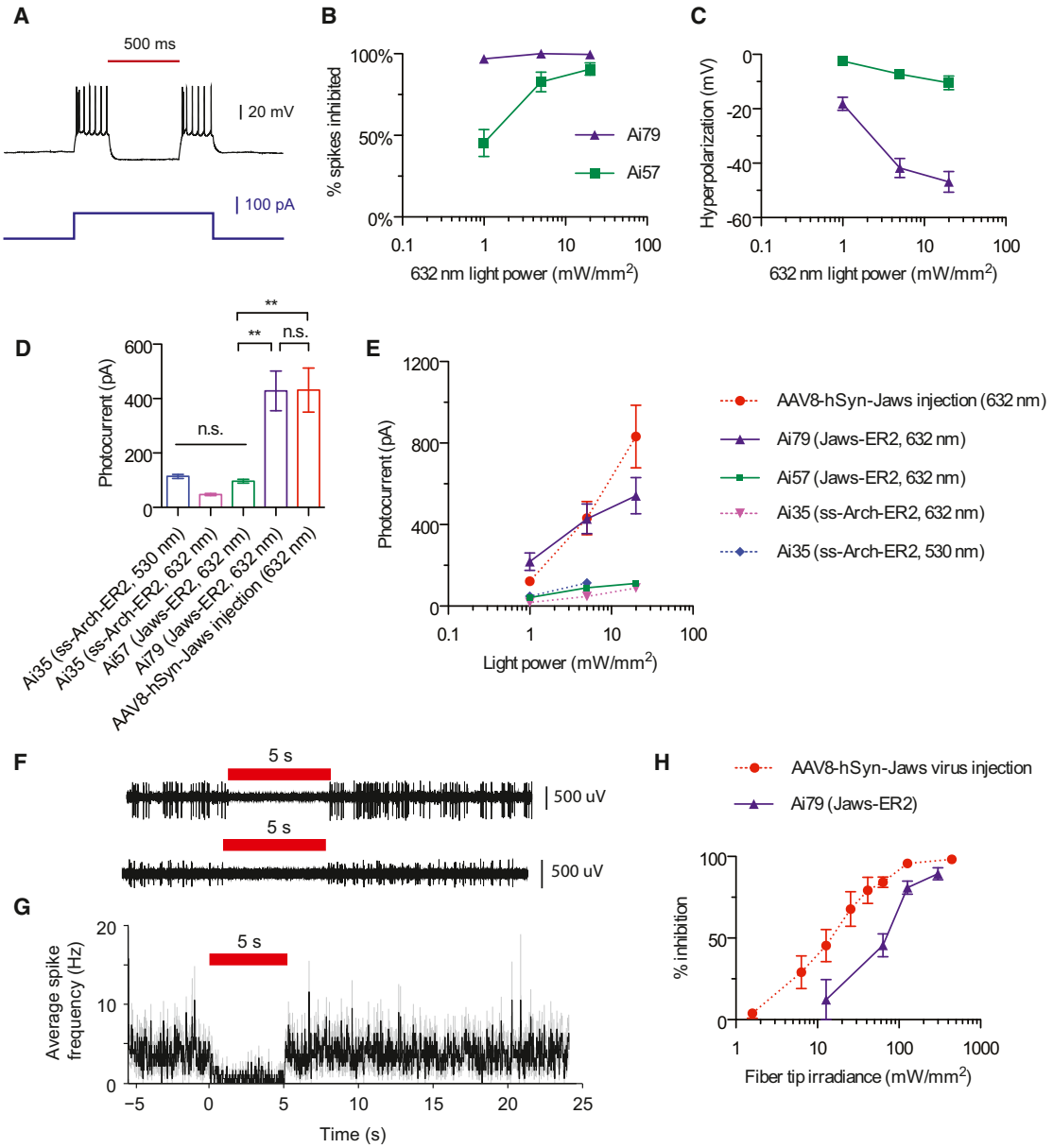

Figure 8. Optogenetic Inhibition of Neural Activity in Reporter Lines Expressing Jaws

(A) Representative current-clamp recording of a Jaws-expressing neuron from Ai79 undergoing optically evoked (632 nm, 5 mW/mm^2) hyperpolarization in an acute cortical slice.

(B) Comparison of red light-induced inhibition of electrically evoked spiking in slices from Ai79 and Ai57 mice. Spiking was induced by a current injection of 1.5× the rheobase.

(C) Comparison of red light-induced hyperpolarization in slices from Ai79 and Ai57 mice.

(D) Comparison of red or green light (632 or 530 nm, 5 mW/mm^2)-induced photocurrents in slices from Ai79, Ai57, Ai35, and AAV-Jaws virus-injected mice.

(E) Comparison of light-induced photocurrents in slices from Ai79, Ai57, Ai35, and AAV-Jaws virus-injected mice across different light intensities for red or green light.

(F and G) Representative extracellular recordings (F) in awake Ai79 mice demonstrate the in vivo inhibition of spontaneous firing activities (G) of Jaws-expressing neurons.

(H) Comparison of in vivo inhibition of spontaneous firing activities over a range of red light intensities between Ai79 and AAV-Jaws-injected mice. All values represent mean ± SEM. **p < 0.01; n.s., not significant. (See also Figure S9.)

Besides the intersectional strategies already shown here, we also tested additional recombinases B3 and KD and the Gal4/UAS transcriptional activation system but obtained undesirable outcomes (see Table S2). However, there are still other approaches with unique merits that we have not tested, such as split-Cre (Casanova et al., 2003; Hirrlinger et al., 2009; Wang

et al., 2012) or the creation of Flp-, Dre-, or tTA-dependent Cre driver lines, which could be applied to the many existing floxed alleles. Developing these alternative intersectional approaches will further expand our capability in cell-type-specific control.

The validated transgenic strategies and new transgenic lines reported here will probably benefit a variety of applications. More Flpo, Dre, and tTA driver lines can be generated that, in conjunction with Cre driver lines, enable the targeting to highly specific cell types and populations. The dual-driver approaches allow for not only an "A and B" type of intersection, but also for other types of simultaneous differential control, such as "A or B" or "A not B" (Fenno et al., 2014; Huang and Zeng, 2013), when appropriate double reporter mice or viruses are developed. Even the low-level promiscuous recombination of Cre on Rox sites can be used to create extremely sparse labeling of individual cells by combining Rox-stop-Rox reporters with Cre drivers. An issue with using intersectional transgenic strategies is the laborious breeding involved in generating triple Tg mice. We found that both Rosa26 and TIGRE homozygous Tg mice are fertile, and because all these are knockin alleles, PCR-genotyping methods can be designed to distinguish wild-type, heterozygous, and homozygous alleles. So using homozygous alleles and/or double Tg × double Tg breeding schemes will increase breeding efficiency.

The collection of reporter lines should facilitate various ways of observing and manipulating cell-type functions, having advantage over viral expressions in large-area, uniform, and long-term monitoring and manipulation of neuronal activities. In particular, stable transgenic expression of GCaMP6f and GCaMP6s (Ai93-96 and Snap25-2A-GCaMP6s), YCX2.60 (Ai92), VSFPB (Ai78), and iGluSnFR (Ai85; Tim Murphy and H.Z., unpublished data) provides various options of imaging neuronal activity with increased sensitivity, complementing other recently reported transgenic lines PC::G5-tdT (Gee et al., 2014) and Thy1-GCaMP6 (Dana et al., 2014). These examples indicate that the TIGRE platform is suitable for expressing existing or new genetic tools and thus expanding the arsenal of genetic approaches to further our understanding of diverse biological systems.

EXPERIMENTAL PROCEDURES

All experimental procedures related to the use of mice were conducted according to NIH guidelines, the UK Animals Scientific Procedures Act (1986), the guidelines of the Veterinary Office of Switzerland, and the New Zealand Animal Welfare Act (1999). Experiments performed at the Allen Institute were approved by the Institutional Animal Care and Use Committee (IACUC) of the Allen Institute for Brain Science. Experiments performed at University College London were under personal and project licenses released by the Home Office following appropriate ethics review. Experiments performed at the University of Zurich were approved by the Cantonal Veterinary Office in Zurich. Additional details of experimental procedures are available in Supplemental Experimental Procedures online.

Transgenic Mice Generation and Expression Characterization

Transgenic mice were generated by inserting transgene cassettes into endogenous genomic loci via homologous recombination as previously described (Madisen et al., 2010) and, in many cases, subsequent Flp-mediated RMCE. Expression of the reporter genes was assessed by epifluorescence or laser-scanning confocal imaging of native fluorescence (without antibody staining), by FACS of single-cell suspensions or by ISH. All ISH data can be found at the Transgenic Characterization database (http://connectivity.brain-map.org/transgenic/search/basic).

In Vitro and In Vivo Wide-Field Voltage Imaging

Hippocampal slice recording was done at room temperature. The dentate gyrus was imaged with a cooled CCD camera. In vivo imaging was done through thinned skull of head-fixed animal allowed to move freely on a spherical treadmill. Stimuli were trains of visual, somatosensory, or auditory stimuli, delivered to elicit periodic responses in cortex.

In Vivo Two-Photon Calcium Imaging

In visual cortex imaging experiments, the animal was allowed to move freely on a rotatable disc while head fixed. Visual stimuli consisted of drifting sinusoidal gratings with varying spatial frequencies, temporal frequencies, and orientations. In somatosensory cortex imaging experiments, mice were anesthetized and neuronal responses were measured in layer 2/3 upon mechanical stimulation of the identified principal whisker. Image data were acquired using custom-built two-photon microscopes with resonant and galvanometric scanners.

In Vitro and In Vivo Electrophysiology of Optogenetic Silencing

In vivo extracellular recordings were conducted in the visual cortex of awake, head-fixed mice using a glass microelectrode attached with a 200-μm diameter optical fiber that is coupled to a 637-nm laser. Whole-cell patch-clamp recording in slice was carried out at 32°C with added Picrotoxin and kynurenic acid in ACSF to block GABAergic and glutamatergic synaptic transmission. Light pulses were delivered through the objective lens using a 530-nm LED or a 625-nm LED plus a 632 ± 11 nm filter.

ACCESSION NUMBERS

The DDBJ/EMBL/GenBank accession number for the sequence of YCX2.60 reported in this paper is LC025957.

SUPPLEMENTAL INFORMATION

Supplemental Information includes Supplemental Experimental Procedures, nine figures, two tables, and four movies and can be found with this article online at http://dx.doi.org/10.1016/j.neuron.2015.02.022.

AUTHOR CONTRIBUTIONS

L.M. and H.Z. designed the transgenic strategies. L.M., H.G., and M.M. generated all new transgenic mouse lines except Nr4a2-SA-IR-Dre and some of the AAVs. C.M. and A.N. generated the Nr4a2-SA-IR-Dre mouse line. D.S., A.B., T.K., and M.C. conducted in vivo wide-field voltage imaging on Ai78 mice. R.M.E. conducted slice physiology on Ai78 mice. A.R.G., A.C., and R.C.R. conducted in vivo two-photon calcium imaging on Ai93 and Ai95 mice. A.v.d.B., L.E., and F.H. conducted in vivo two-photon calcium imaging on Ai92 mice. N.C.K., A.S.C., L.L., and E.S.B. conducted optogenetic silencing studies on Ai35, Ai57, and Ai79 mice. Y.N. and A.M. developed YCX2.60. B.T. and T.N.N. conducted FACS analysis and made some of the AAVs. S.M.S. provided project management for this work. L.M., A.R.G., D.S., A.S.C., L.L., R.M.E., T.K., M.C., and H.Z. were main contributors to data analysis and manuscript writing, with input from other co-authors.

ACKNOWLEDGMENTS

We are grateful to the Research and Development, Structured Science and Technology teams at the Allen Institute for their technical support in stereotaxic injections, mouse colony management, and ISH gene expression characterization. We thank Robert Hunter for coordinating transgenic mice production and Charu Reddy and Wolfgang Omlor for technical support. We thank Douglas Kim for providing the GCaMP6f and GCaMP6s constructs, Loren Looger for providing the iGluSnFR construct, Gary Felsenfeld for providing the chicken β-globin HS4 insulator element construct, Philippe

Soriano for providing the FLPo construct via Addgene, and Anton Maximov for providing the DHFR-Cre construct. This work was funded by the Allen Institute for Brain Science, NIH grant MH085500 to H.Z. and A.N., NIH grant DA028298 to H.Z., and Wellcome Trust grant 095669 to M.C. M.C. holds the GlaxoSmithKline / Fight for Sight Chair in Visual Neuroscience. The authors wish to thank the Allen Institute founders, Paul G. Allen and Jody Allen, for their vision, encouragement, and support.

Received: August 25, 2014
Revised: January 8, 2015
Accepted: February 11, 2015
Published: March 4, 2015

REFERENCES

Ackman, J.B., Burbridge, T.J., and Crair, M.C. (2012). Retinal waves coordinate patterned activity throughout the developing visual system. Nature *490*, 219–225.

Akemann, W., Mutoh, H., Perron, A., Park, Y.K., Iwamoto, Y., and Knöpfel, T. (2012). Imaging neural circuit dynamics with a voltage-sensitive fluorescent protein. J. Neurophysiol. *108*, 2323–2337.

Anastassiadis, K., Fu, J., Patsch, C., Hu, S., Weidlich, S., Duerschke, K., Buchholz, F., Edenhofer, F., and Stewart, A.F. (2009). Dre recombinase, like Cre, is a highly efficient site-specific recombinase in E. coli, mammalian cells and mice. Dis. Model. Mech. *2*, 508–515.

Andermann, M.L., Kerlin, A.M., Roumis, D.K., Glickfeld, L.L., and Reid, R.C. (2011). Functional specialization of mouse higher visual cortical areas. Neuron *72*, 1025–1039.

Arenkiel, B.R., Peca, J., Davison, I.G., Feliciano, C., Deisseroth, K., Augustine, G.J., Ehlers, M.D., and Feng, G. (2007). In vivo light-induced activation of neural circuitry in transgenic mice expressing channelrhodopsin-2. Neuron *54*, 205–218.

Benucci, A., Frazor, R.A., and Carandini, M. (2007). Standing waves and traveling waves distinguish two circuits in visual cortex. Neuron *55*, 103–117.

Bonin, V., Histed, M.H., Yurgenson, S., and Reid, R.C. (2011). Local diversity and fine-scale organization of receptive fields in mouse visual cortex. J. Neurosci. *31*, 18506–18521.

Buchholz, F., Angrand, P.O., and Stewart, A.F. (1998). Improved properties of FLP recombinase evolved by cycling mutagenesis. Nat. Biotechnol. *16*, 657–662.

Carandini, M., Shimaoka, D., Rossi, L.F., Sato, T.K., Benucci, A., and Knöpfel, T. (2015). Imaging the awake visual cortex with a genetically encoded voltage indicator. J. Neurosci. *35*, 53–63.

Casanova, E., Lemberger, T., Fehsenfeld, S., Mantamadiotis, T., and Schütz, G. (2003). Alpha complementation in the Cre recombinase enzyme. Genesis *37*, 25–29.

Chen, T.W., Wardill, T.J., Sun, Y., Pulver, S.R., Renninger, S.L., Baohan, A., Schreiter, E.R., Kerr, R.A., Orger, M.B., Jayaraman, V., et al. (2013). Ultrasensitive fluorescent proteins for imaging neuronal activity. Nature *499*, 295–300.

Chung, J.H., Bell, A.C., and Felsenfeld, G. (1997). Characterization of the chicken beta-globin insulator. Proc. Natl. Acad. Sci. USA *94*, 575–580.

Chuong, A.S., Miri, M.L., Busskamp, V., Matthews, G.A., Acker, L.C., Sørensen, A.T., Young, A., Klapoetke, N.C., Henninger, M.A., Kodandaramaiah, S.B., et al. (2014). Noninvasive optical inhibition with a red-shifted microbial rhodopsin. Nat. Neurosci. *17*, 1123–1129.

Dana, H., Chen, T.W., Hu, A., Shields, B.C., Guo, C., Looger, L.L., Kim, D.S., and Svoboda, K. (2014). Thy1-GCaMP6 transgenic mice for neuronal population imaging in vivo. PLoS ONE *9*, e108697.

Dymecki, S.M., and Kim, J.C. (2007). Molecular neuroanatomy's "Three Gs": a primer. Neuron *54*, 17–34.

Dymecki, S.M., Ray, R.S., and Kim, J.C. (2010). Mapping cell fate and function using recombinase-based intersectional strategies. Methods Enzymol. *477*, 183–213.

Feng, G., Mellor, R.H., Bernstein, M., Keller-Peck, C., Nguyen, Q.T., Wallace, M., Nerbonne, J.M., Lichtman, J.W., and Sanes, J.R. (2000). Imaging neuronal subsets in transgenic mice expressing multiple spectral variants of GFP. Neuron *28*, 41–51.

Fenno, L., Yizhar, O., and Deisseroth, K. (2011). The development and application of optogenetics. Annu. Rev. Neurosci. *34*, 389–412.

Fenno, L.E., Mattis, J., Ramakrishnan, C., Hyun, M., Lee, S.Y., He, M., Tucciarone, J., Selimbeyoglu, A., Berndt, A., Grosenick, L., et al. (2014). Targeting cells with single vectors using multiple-feature Boolean logic. Nat. Methods *11*, 763–772.

Garner, A.R., Rowland, D.C., Hwang, S.Y., Baumgaertel, K., Roth, B.L., Kentros, C., and Mayford, M. (2012). Generation of a synthetic memory trace. Science *335*, 1513–1516.

Gaszner, M., and Felsenfeld, G. (2006). Insulators: exploiting transcriptional and epigenetic mechanisms. Nat. Rev. Genet. *7*, 703–713.

Gee, J.M., Smith, N.A., Fernandez, F.R., Economo, M.N., Brunert, D., Rothermel, M., Morris, S.C., Talbot, A., Palumbos, S., Ichida, J.M., et al. (2014). Imaging activity in neurons and glia with a Polr2a-based and cre-dependent GCaMP5G-IR-tdTomato reporter mouse. Neuron *83*, 1058–1072.

Gerfen, C.R., Paletzki, R., and Heintz, N. (2013). GENSAT BAC cre-recombinase driver lines to study the functional organization of cerebral cortical and basal ganglia circuits. Neuron *80*, 1368–1383.

Gong, S., Doughty, M., Harbaugh, C.R., Cummins, A., Hatten, M.E., Heintz, N., and Gerfen, C.R. (2007). Targeting Cre recombinase to specific neuron populations with bacterial artificial chromosome constructs. J. Neurosci. *27*, 9817–9823.

Gossen, M., and Bujard, H. (1992). Tight control of gene expression in mammalian cells by tetracycline-responsive promoters. Proc. Natl. Acad. Sci. USA *89*, 5547–5551.

Gradinaru, V., Zhang, F., Ramakrishnan, C., Mattis, J., Prakash, R., Diester, I., Goshen, I., Thompson, K.R., and Deisseroth, K. (2010). Molecular and cellular approaches for diversifying and extending optogenetics. Cell *141*, 154–165.

Hackett, T.A., Barkat, T.R., O'Brien, B.M., Hensch, T.K., and Polley, D.B. (2011). Linking topography to tonotopy in the mouse auditory thalamocortical circuit. J. Neurosci. *31*, 2983–2995.

Haddad, R., Lanjuin, A., Madisen, L., Zeng, H., Murthy, V.N., and Uchida, N. (2013). Olfactory cortical neurons read out a relative time code in the olfactory bulb. Nat. Neurosci. *16*, 949–957.

Harris, J.A., Hirokawa, K.E., Sorensen, S.A., Gu, H., Mills, M., Ng, L.L., Bohn, P., Mortrud, M., Ouellette, B., Kidney, J., et al. (2014). Anatomical characterization of Cre driver mice for neural circuit mapping and manipulation. Front. Neural Circuits *8*, 76.

Hirrlinger, J., Scheller, A., Hirrlinger, P.G., Kellert, B., Tang, W., Wehr, M.C., Goebbels, S., Reichenbach, A., Sprengel, R., Rossner, M.J., and Kirchhoff, F. (2009). Split-cre complementation indicates coincident activity of different genes in vivo. PLoS ONE *4*, e4286.

Horikawa, K., Yamada, Y., Matsuda, T., Kobayashi, K., Hashimoto, M., Matsuura, T., Miyawaki, A., Michikawa, T., Mikoshiba, K., and Nagai, T. (2010). Spontaneous network activity visualized by ultrasensitive Ca(2+) indicators, yellow Cameleon-Nano. Nat. Methods *7*, 729–732.

Huang, Z.J., and Zeng, H. (2013). Genetic approaches to neural circuits in the mouse. Annu. Rev. Neurosci. *36*, 183–215.

Issa, J.B., Haeffele, B.D., Agarwal, A., Bergles, D.E., Young, E.D., and Yue, D.T. (2014). Multiscale optical Ca2+ imaging of tonal organization in mouse auditory cortex. Neuron *83*, 944–959.

Iurilli, G., Ghezzi, D., Olcese, U., Lassi, G., Nazzaro, C., Tonini, R., Tucci, V., Benfenati, F., and Medini, P. (2012). Sound-driven synaptic inhibition in primary visual cortex. Neuron *73*, 814–828.

Iyer, M., Wu, L., Carey, M., Wang, Y., Smallwood, A., and Gambhir, S.S. (2001). Two-step transcriptional amplification as a method for imaging reporter gene expression using weak promoters. Proc. Natl. Acad. Sci. USA *98*, 14595–14600.

Jackman, S.L., Beneduce, B.M., Drew, I.R., and Regehr, W.G. (2014). Achieving high-frequency optical control of synaptic transmission. J. Neurosci. *34*, 7704–7714.

Kheirbek, M.A., Drew, L.J., Burghardt, N.S., Costantini, D.O., Tannenholz, L., Ahmari, S.E., Zeng, H., Fenton, A.A., and Hen, R. (2013). Differential control of learning and anxiety along the dorsoventral axis of the dentate gyrus. Neuron *77*, 955–968.

Kirkcaldie, M.T.K. (2012). Neocortex. In The Mouse Nervous System, C. Watson, G. Paxinos, and L. Puelles, eds. (San Diego, CA: Academic Press), pp. 52–111.

Knöpfel, T. (2012). Genetically encoded optical indicators for the analysis of neuronal circuits. Nat. Rev. Neurosci. *13*, 687–700.

Kranz, A., Fu, J., Duerschke, K., Weidlich, S., Naumann, R., Stewart, A.F., and Anastassiadis, K. (2010). An improved Flp deleter mouse in C57Bl/6 based on Flpo recombinase. Genesis *48*, 512–520.

Lee, S.H., Marchionni, I., Bezaire, M., Varga, C., Danielson, N., Lovett-Barron, M., Losonczy, A., and Soltesz, I. (2014). Parvalbumin-positive basket cells differentiate among hippocampal pyramidal cells. Neuron *82*, 1129–1144.

Li, L., Tasic, B., Micheva, K.D., Ivanov, V.M., Spletter, M.L., Smith, S.J., and Luo, L. (2010). Visualizing the distribution of synapses from individual neurons in the mouse brain. PLoS ONE *5*, e11503.

Madisen, L., Zwingman, T.A., Sunkin, S.M., Oh, S.W., Zariwala, H.A., Gu, H., Ng, L.L., Palmiter, R.D., Hawrylycz, M.J., Jones, A.R., et al. (2010). A robust and high-throughput Cre reporting and characterization system for the whole mouse brain. Nat. Neurosci. *13*, 133–140.

Madisen, L., Mao, T., Koch, H., Zhuo, J.M., Berenyi, A., Fujisawa, S., Hsu, Y.W., Garcia, A.J., 3rd, Gu, X., Zanella, S., et al. (2012). A toolbox of Cre-dependent optogenetic transgenic mice for light-induced activation and silencing. Nat. Neurosci. *15*, 793–802.

Marvin, J.S., Borghuis, B.G., Tian, L., Cichon, J., Harnett, M.T., Akerboom, J., Gordus, A., Renninger, S.L., Chen, T.W., Bargmann, C.I., et al. (2013). An optimized fluorescent probe for visualizing glutamate neurotransmission. Nat. Methods *10*, 162–170.

Mayford, M., Bach, M.E., Huang, Y.Y., Wang, L., Hawkins, R.D., and Kandel, E.R. (1996). Control of memory formation through regulated expression of a CaMKII transgene. Science *274*, 1678–1683.

Muzumdar, M.D., Tasic, B., Miyamichi, K., Li, L., and Luo, L. (2007). A global double-fluorescent Cre reporter mouse. Genesis *45*, 593–605.

Nagai, T., Yamada, S., Tominaga, T., Ichikawa, M., and Miyawaki, A. (2004). Expanded dynamic range of fluorescent indicators for Ca(2+) by circularly permuted yellow fluorescent proteins. Proc. Natl. Acad. Sci. USA *101*, 10554–10559.

Nguyen-Vu, T.D., Kimpo, R.R., Rinaldi, J.M., Kohli, A., Zeng, H., Deisseroth, K., and Raymond, J.L. (2013). Cerebellar Purkinje cell activity drives motor learning. Nat. Neurosci. *16*, 1734–1736.

Petersen, R.P., Moradpour, F., Eadie, B.D., Shin, J.D., Kannangara, T.S., Delaney, K.R., and Christie, B.R. (2013). Electrophysiological identification of medial and lateral perforant path inputs to the dentate gyrus. Neuroscience *252*, 154–168.

Pi, H.J., Hangya, B., Kvitsiani, D., Sanders, J.I., Huang, Z.J., and Kepecs, A. (2013). Cortical interneurons that specialize in disinhibitory control. Nature *503*, 521–524.

Ray, R.S., Corcoran, A.E., Brust, R.D., Kim, J.C., Richerson, G.B., Nattie, E., and Dymecki, S.M. (2011). Impaired respiratory and body temperature control upon acute serotonergic neuron inhibition. Science *333*, 637–642.

Raymond, C.S., and Soriano, P. (2007). High-efficiency FLP and PhiC31 site-specific recombination in mammalian cells. PLoS ONE *2*, e162.

Reijmers, L.G., Perkins, B.L., Matsuo, N., and Mayford, M. (2007). Localization of a stable neural correlate of associative memory. Science *317*, 1230–1233.

Robertson, S.D., Plummer, N.W., de Marchena, J., and Jensen, P. (2013). Developmental origins of central norepinephrine neuron diversity. Nat. Neurosci. *16*, 1016–1023.

Sauer, B., and McDermott, J. (2004). DNA recombination with a heterospecific Cre homolog identified from comparison of the pac-c1 regions of P1-related phages. Nucleic Acids Res. *32*, 6086–6095.

Scott, G., Fagerholm, E.D., Mutoh, H., Leech, R., Sharp, D.J., Shew, W.L., and Knöpfel, T. (2014). Voltage imaging of waking mouse cortex reveals emergence of critical neuronal dynamics. J. Neurosci. *34*, 16611–16620.

Taniguchi, H., He, M., Wu, P., Kim, S., Paik, R., Sugino, K., Kvitsiani, D., Fu, Y., Lu, J., Lin, Y., et al. (2011). A resource of Cre driver lines for genetic targeting of GABAergic neurons in cerebral cortex. Neuron *71*, 995–1013.

Tasic, B., Miyamichi, K., Hippenmeyer, S., Dani, V.S., Zeng, H., Joo, W., Zong, H., Chen-Tsai, Y., and Luo, L. (2012). Extensions of MADM (mosaic analysis with double markers) in mice. PLoS ONE *7*, e33332.

Urlinger, S., Baron, U., Thellmann, M., Hasan, M.T., Bujard, H., and Hillen, W. (2000). Exploring the sequence space for tetracycline-dependent transcriptional activators: novel mutations yield expanded range and sensitivity. Proc. Natl. Acad. Sci. USA *97*, 7963–7968.

Wang, Q., and Burkhalter, A. (2007). Area map of mouse visual cortex. J. Comp. Neurol. *502*, 339–357.

Wang, L., Sharma, K., Deng, H.X., Siddique, T., Grisotti, G., Liu, E., and Roos, R.P. (2008). Restricted expression of mutant SOD1 in spinal motor neurons and interneurons induces motor neuron pathology. Neurobiol. Dis. *29*, 400–408.

Wang, P., Chen, T., Sakurai, K., Han, B.X., He, Z., Feng, G., and Wang, F. (2012). Intersectional Cre driver lines generated using split-intein mediated split-Cre reconstitution. Sci. Rep. *2*, 497.

Yamada, Y., Michikawa, T., Hashimoto, M., Horikawa, K., Nagai, T., Miyawaki, A., Häusser, M., and Mikoshiba, K. (2011). Quantitative comparison of genetically encoded Ca indicators in cortical pyramidal cells and cerebellar Purkinje cells. Front. Cell. Neurosci. *5*, 18.

Zariwala, H.A., Borghuis, B.G., Hoogland, T.M., Madisen, L., Tian, L., De Zeeuw, C.I., Zeng, H., Looger, L.L., Svoboda, K., and Chen, T.W. (2012). A Cre-dependent GCaMP3 reporter mouse for neuronal imaging in vivo. J. Neurosci. *32*, 3131–3141.

Zeng, H., and Madisen, L. (2012). Mouse transgenic approaches in optogenetics. Prog. Brain Res. *196*, 193–213.

Zeng, H., Horie, K., Madisen, L., Pavlova, M.N., Gragerova, G., Rohde, A.D., Schimpf, B.A., Liang, Y., Ojala, E., Kramer, F., et al. (2008). An inducible and reversible mouse genetic rescue system. PLoS Genet. *4*, e1000069.

Zhao, S., Cunha, C., Zhang, F., Liu, Q., Gloss, B., Deisseroth, K., Augustine, G.J., and Feng, G. (2008). Improved expression of halorhodopsin for light-induced silencing of neuronal activity. Brain Cell Biol. *36*, 141–154.

Zhao, S., Ting, J.T., Atallah, H.E., Qiu, L., Tan, J., Gloss, B., Augustine, G.J., Deisseroth, K., Luo, M., Graybiel, A.M., and Feng, G. (2011). Cell type–specific channelrhodopsin-2 transgenic mice for optogenetic dissection of neural circuitry function. Nat. Methods *8*, 745–752.

Zhu, P., Aller, M.I., Baron, U., Cambridge, S., Bausen, M., Herb, J., Sawinski, J., Cetin, A., Osten, P., Nelson, M.L., et al. (2007). Silencing and un-silencing of tetracycline-controlled genes in neurons. PLoS ONE *2*, e533.

Neuron

Supplemental Information

Transgenic Mice for Intersectional Targeting of Neural Sensors and Effectors with High Specificity and Performance

Linda Madisen, Aleena R. Garner, Daisuke Shimaoka, Amy S. Chuong, Nathan C. Klapoetke, Lu Li, Alexander van der Bourg, Yusuke Niino, Ladan Egolf, Claudio Monetti, Hong Gu, Maya Mills, Adrian Cheng, Bosiljka Tasic, Thuc Nghi Nguyen, Susan M. Sunkin, Andrea Benucci, Andras Nagy, Atsushi Miyawaki, Fritjof Helmchen, Ruth M. Empson, Thomas Knöpfel, Edward S. Boyden, R. Clay Reid, Matteo Carandini, and Hongkui Zeng

SUPPLEMENTAL DATA

Inventory:

Figure S1

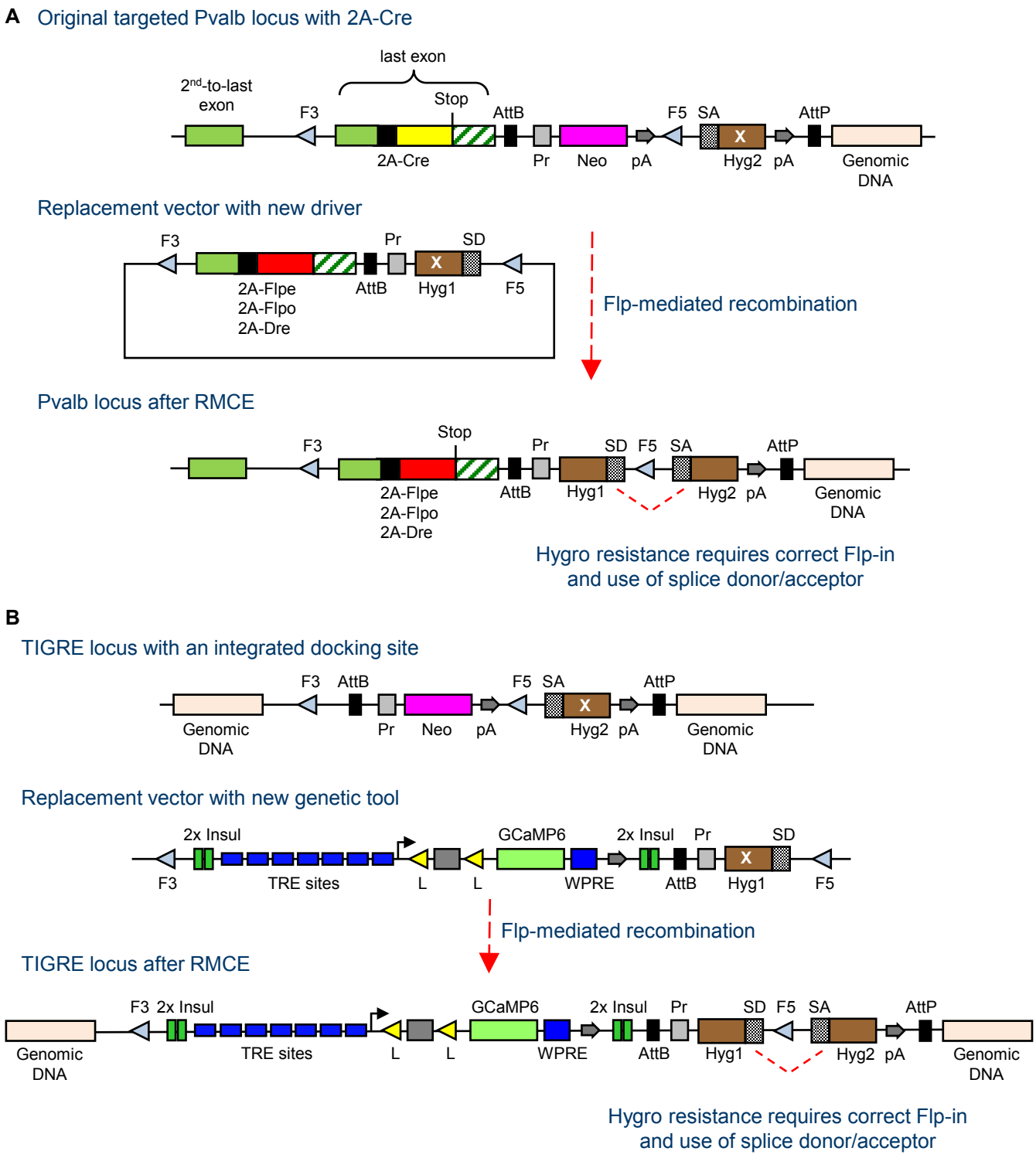
A
Original targeted Pvalb locus with 2A-Cre
last exon
2nd-to-last exon
Stop
F3
AttB
F5
SA
AttP
2A-Cre
Pr
Neo
pA
X
Hyg2
pA
Genomic DNA
Replacement vector with new driver
F3
Pr
SD
2A-Flpe
2A-Flpo
2A-Dre
AttB
Hyg1
F5
Flp-mediated recombination
Pvalb locus after RMCE
Stop
F3
Pr
SD
F5
SA
AttP
2A-Flpe
2A-Flpo
2A-Dre
AttB
Hyg1
Hyg2
pA
Genomic DNA
Hygro resistance requires correct Flp-in and use of splice donor/acceptor
B
TIGRE locus with an integrated docking site
F3
AttB
F5
SA
AttP
Genomic DNA
Pr
Neo
pA
X
Hyg2
pA
Genomic DNA
Replacement vector with new genetic tool
2x Insul
GCaMP6
2x Insul
Pr
SD
F3
TRE sites
L
L
WPRE
AttB
Hyg1
F5
Flp-mediated recombination
TIGRE locus after RMCE
F3
2x Insul
GCaMP6
2x Insul
Pr
SD
F5
SA
AttP
Genomic DNA
TRE sites
L
L
WPRE
AttB
Hyg1
Hyg2
pA
Genomic DNA
Hygro resistance requires correct Flp-in and use of splice donor/acceptor

Figure S1. Recombinase-mediated cassette exchange (RMCE) strategy for inserting new transgenes into the *Pvalb* locus or the TIGRE locus. (Related to **Figures 1** and **3**.) Our RMCE strategy is based on Flp-mediated recombination of FRT3 (F3) and FRT5 (F5) target sites, thus the process is also called "Flp-in". (**A**) RMCE in the *Pvalb* locus. The *Pvalb* locus was originally targeted by homologous recombination to insert T2A-Cre at the endogenous stop codon (top). This ES clone was used in subsequent RMCE experiments to replace T2A-Cre with other driver gene cassettes, including T2A-Flpe, T2A-Flpo, or T2A-Dre. To do this, the originally targeted Pvalb-2A-Cre ES clone is co-transfected with a Flp expression plasmid and a replacement vector containing the modified exon with the new driver (middle). F3 and F5 sites are incompatible with each other, so there is no recombination between them. In the presence of Flp, F3 and F5 each undergoes homophilic recombination, *i.e.* between the F3 (or F5) in the genomic locus and the F3 (or F5) in the replacement vector, leading to the replacement of the DNA segment between F3 and F5 in the genomic locus with that from the replacement vector. Successful cassette exchange joins Hyg1 and Hyg2 domains through mRNA splicing and reconstitutes an active hygromycin-resistant gene, which can be used for selection of exchange events. Since all of our in-house gene targeting experiments utilize the same targeting vector design shown here, *Pvalb*-like RMCE approach is applicable to other targeted gene loci as well, such as the *Snap25* locus reported here. (**B**) RMCE in the TIGRE locus. The originally targeted TIGRE ES clone, containing a Flp/FRT-based empty docking site integrated into the TIGRE locus (top), is co-transfected with a Flp expression plasmid and a replacement vector containing the transgene cassette of interest (middle). The Flp-in RMCE process is identical to that described in A.

Figure S2

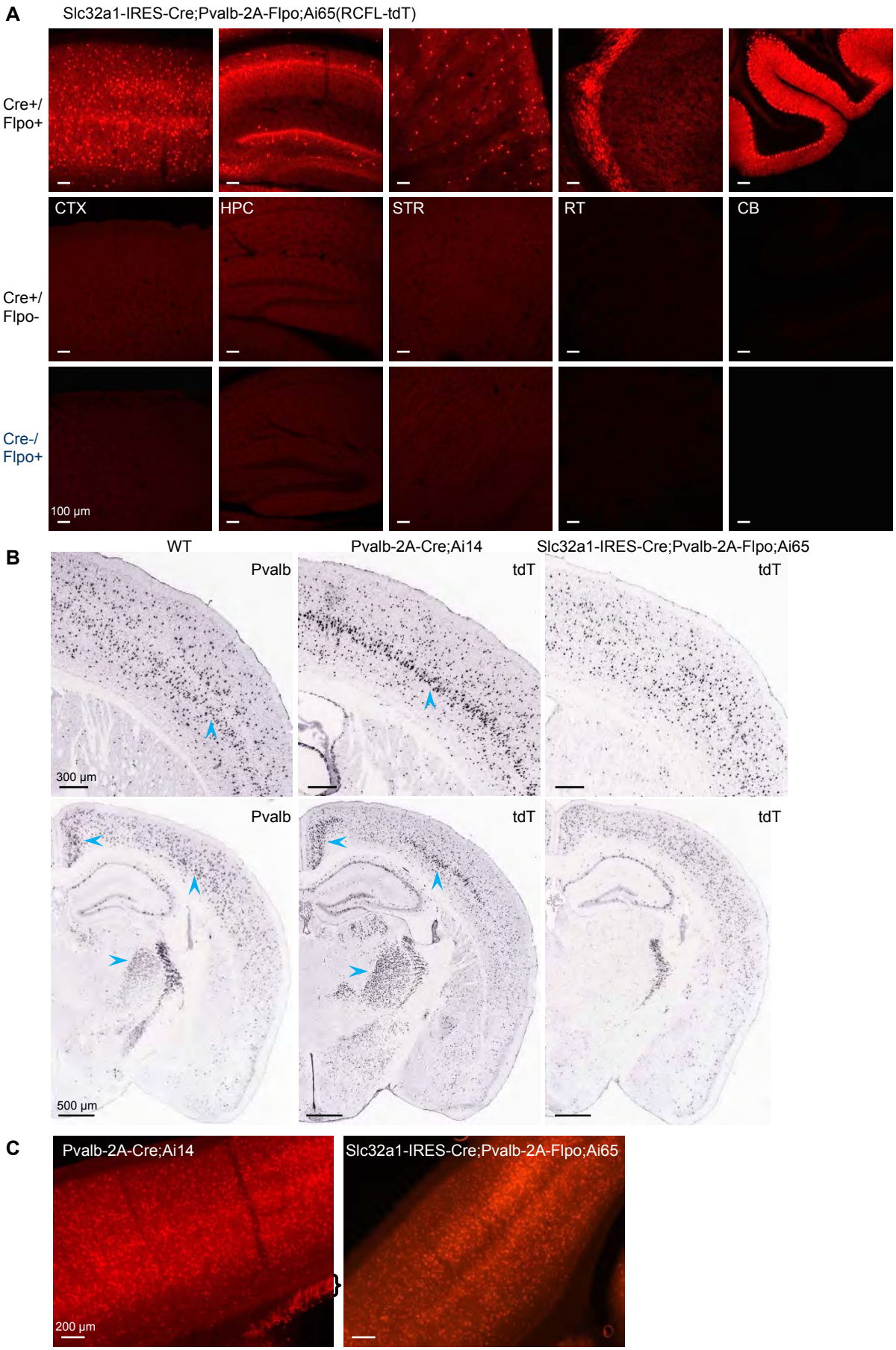
A
Slc32a1-IRES-Cre;Pvalb-2A-Flpo;Ai65(RCFL-tdT)
Cre+/
Flpo+
CTX
HPC
STR
RT
CB
Cre+/
Flpo-
Cre-/
Flpo+
100 μm
B
WT
Pvalb-2A-Cre;Ai14
Slc32a1-IRES-Cre;Pvalb-2A-Flpo;Ai65
Pvalb
tdT
tdT
300 μm
Pvalb
tdT
tdT
500 μm
C
Pvalb-2A-Cre;Ai14
Slc32a1-IRES-Cre;Pvalb-2A-Flpo;Ai65
200 μm

Figure S2. Dual-recombinase intersection using Cre and Flp. (Related to **Figure 1**.) (**A**) Confocal images show that expression of tdTomato reporter in *Slc32a1*+/*Pvalb*+ GABAergic neurons of the Slc32a1-IRES-Cre;Pvalb-2A-Flpo;Ai65 mouse requires both Cre and Flp recombinases. No tdTomato+ cells were found in either Cre+/Flp- or Cre-/Flp+ mouse. CTX, cortex. HPC, hippocampus. STR, striatum. RT, reticular nucleus of the thalamus. CB, cerebellum. (**B**) ISH images comparing the expression pattern of the endogenous *Pvalb* gene with that of the tdTomato reporter gene in the Pvalb-2A-Cre;Ai14 mouse or the Slc32a1-IRES-Cre;Pvalb-2A-Flpo;Ai65 mouse. The endogenous *Pvalb* gene is not only expressed prominently in GABAergic neurons but also at lower levels in excitatory neurons in different parts of the brain, including cortical layer 5 and some nuclei of the thalamus (blue arrow heads, left panels). Consequently, tdTomato reporter is also expressed in these non-GABAergic neurons in the Pvalb-2A-Cre;Ai14 mouse (blue arrow heads, middle panels). No expression in excitatory neurons is observed in the Slc32a1-IRES-Cre;Pvalb-2A-Flpo;Ai65 mouse (right panels). WT, wild-type mouse. (**C**) The presence of cortical excitatory neurons in the Pvalb-2A-Cre;Ai14 mouse can be confirmed by the presence of labeled axon bundles in the white matter, as indicated by the bracket in the left panel. No labeled axon bundles were found in the white matter beneath the cortex in the Slc32a1-IRES-Cre;Pvalb-2A-Flpo;Ai65 mouse (right panel).

Figure S3

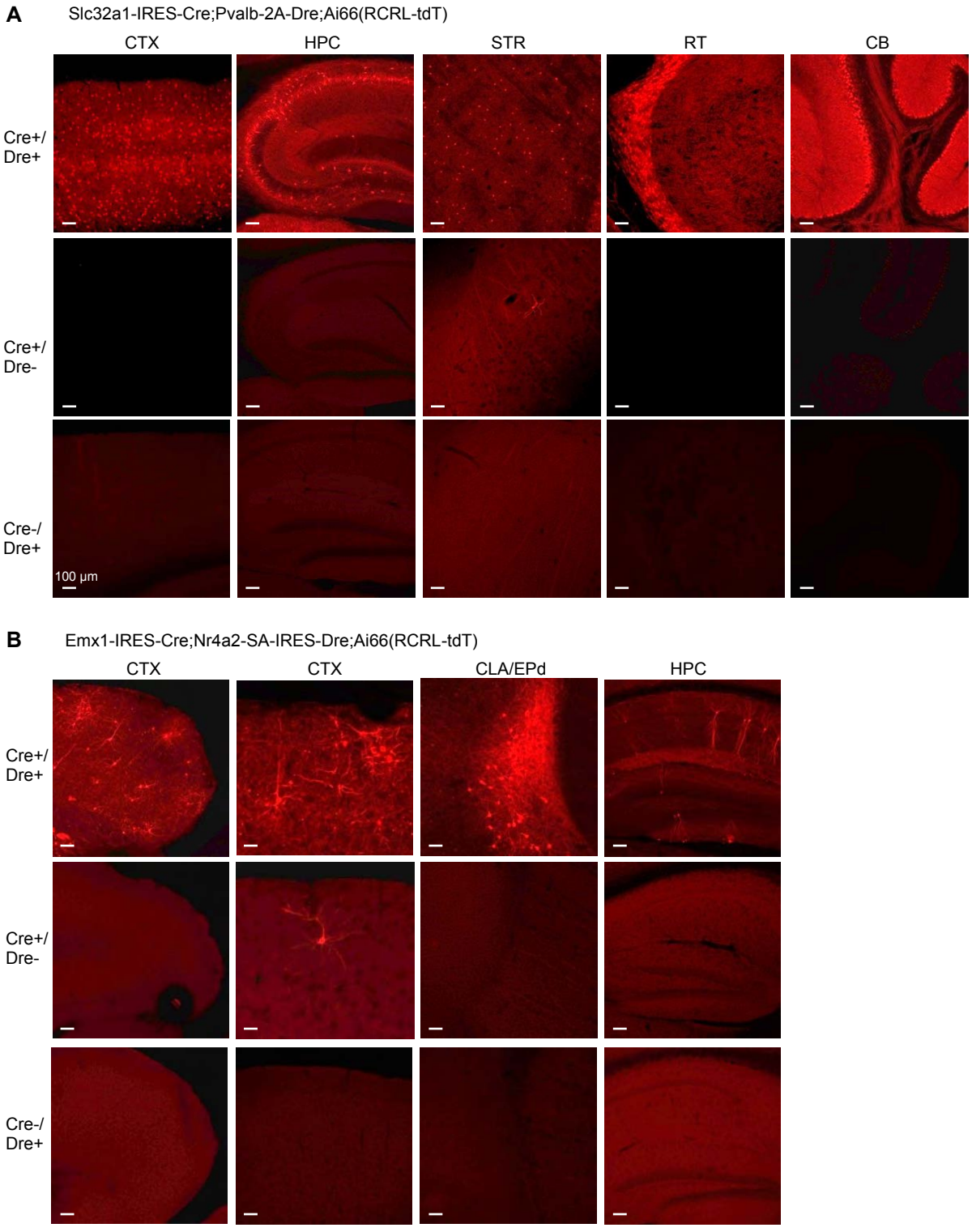
A
Slc32a1-IRES-Cre;Pvalb-2A-Dre;Ai66(RCRL-tdT)
CTX
HPC
STR
RT
CB
Cre+/
Dre+
Cre+/
Dre-
Cre-/
Dre+
100 µm
B
Emx1-IRES-Cre;Nr4a2-SA-IRES-Dre;Ai66(RCRL-tdT)
CTX
CTX
CLA/EPd
HPC
Cre+/
Dre+
Cre+/
Dre-
Cre-/
Dre+

Figure S3. Dual-recombinase intersection using Cre and Dre. (Related to **Figure 1**.) (**A**) Confocal images show that expression of tdTomato reporter in *Slc32a1*+/*Pvalb*+ GABAergic neurons of the Slc32a1-IRES-Cre;Pvalb-2A-Dre;Ai66 mouse requires both Cre and Dre recombinases. Only a couple of tdTomato+ cells were seen in the striatum of Cre+/Dre- mouse. No tdTomato+ cells were found in Cre-/Dre+ mouse. CTX, cortex. HPC, hippocampus. STR, striatum. RT, reticular nucleus of the thalamus. CB, cerebellum. (**B**) Confocal images show that expression of tdTomato reporter in the Emx1-IRES-Cre;Nr4a2-SA-IRES-Dre;Ai66 mouse is restricted to the *Emx1*+/*Nr4a2*+ neurons in the claustrum (CLA) and endopiriform nucleus, dorsal part (EPd), as well as sparsely scattered cells in cortex (CTX) and hippocampus (HPC), where both Cre and Dre are present. No tdTomato+ cells were found in the Cre-/Dre+ mouse. However, a few tdTomato+ cells were found in the Cre+/Dre- mouse, indicating a very low level of promiscuity of Cre activity for recombining the Rox sites.

Figure S4

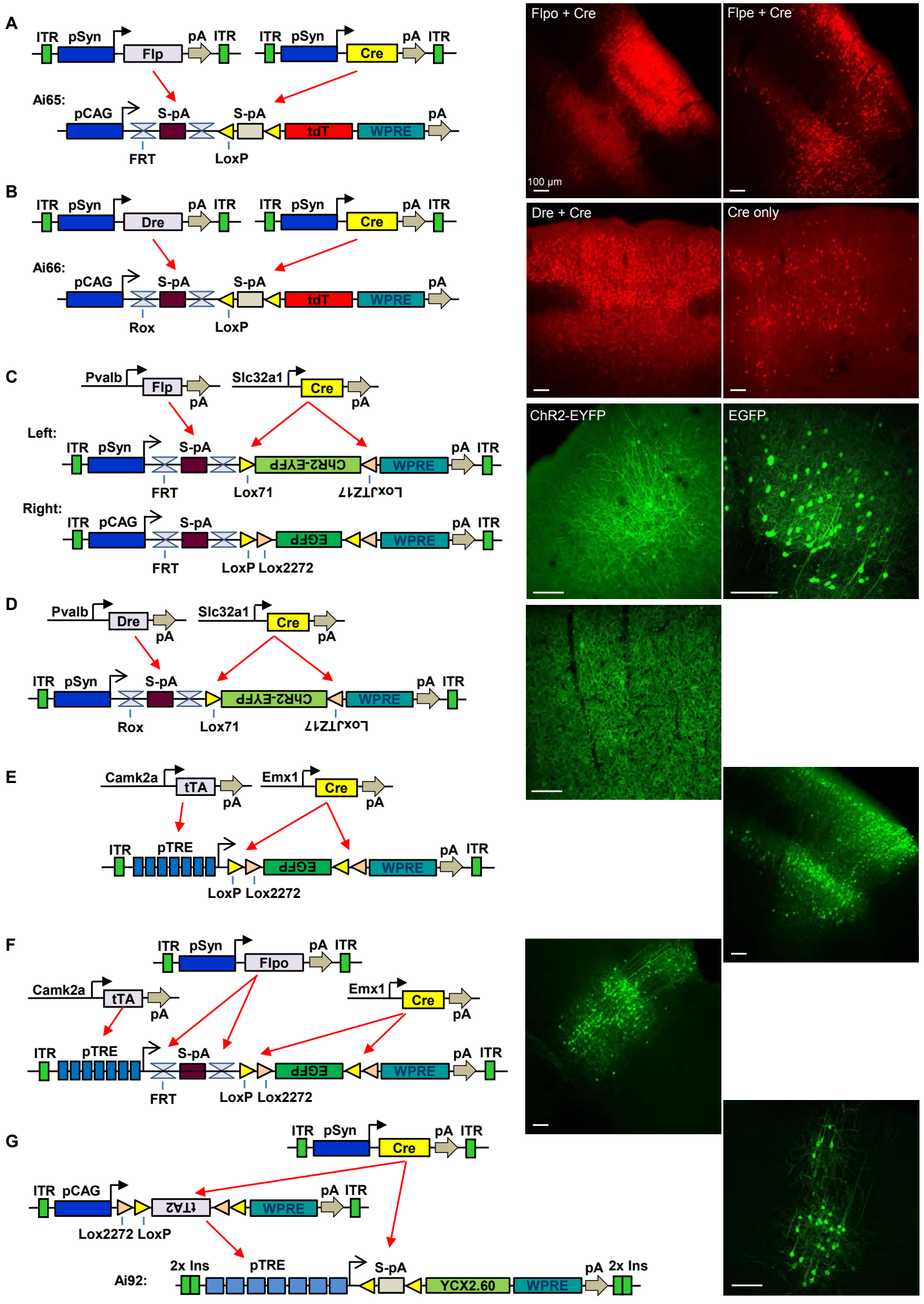
A
ITR pSyn Flp pA ITR
ITR pSyn Cre pA ITR
Ai65:
pCAG S-pA S-pA tdT WPRE pA
FRT LoxP
B
ITR pSyn Dre pA ITR
ITR pSyn Cre pA ITR
Ai66:
pCAG S-pA S-pA tdT WPRE pA
Rox LoxP
C
Pvalb Flp pA
Slc32a1 Cre pA
Left:
ITR pSyn S-pA ChR2-EYFP WPRE pA ITR
FRT Lox71 Lox2272
Right:
ITR pCAG S-pA EGFP WPRE pA ITR
FRT LoxP Lox2272
D
Pvalb Dre pA
Slc32a1 Cre pA
ITR pSyn S-pA ChR2-EYFP WPRE pA ITR
Rox Lox71 Lox2272
E
Camk2a tTA pA
Emx1 Cre pA
ITR pTRE EGFP WPRE pA ITR
LoxP Lox2272
F
ITR pSyn Flpo pA ITR
Camk2a tTA pA
Emx1 Cre pA
ITR pTRE S-pA EGFP WPRE pA ITR
FRT LoxP Lox2272
G
ITR pSyn Cre pA ITR
ITR pCAG tTA2 WPRE pA ITR
Lox2272 LoxP
Ai92:
2x Ins pTRE S-pA YCX2.60 WPRE pA 2x Ins
Flpo + Cre
Flpe + Cre
100 µm
Dre + Cre
Cre only
ChR2-EYFP
EGFP

Figure S4. New recombinant adeno-associated viruses (AAVs) for intersectional strategies. (Related to **Figures 1** and **2**.) (**A-B**) We developed AAVs expressing Cre, Flpe, Flpo or Dre under the Synapsin I promoter (**Table 1**). (**A**) Coinjection of AAV-Cre and AAV-Flpe, or AAV-Cre and AAV-Flpo into Ai65(RCFL-tdT) mice resulted in efficient recombination with AAV-Cre and AAV-Flpo, but with much lower efficiency with AAV-Cre and AAV-Flpe. Single-virus injections of AAV-Cre, AAV-Flpe or AAV-Flpo into Ai65(RCFL-tdT) mice gave no tdT+ cells (data not shown). (**B**) Coinjection of AAV-Cre and AAV-Dre into Ai66(RCRL-tdT) mice resulted in efficient recombination. Single injection of AAV-Cre into Ai66(RCRL-tdT) mice exhibited sparse promiscuous recombination. Single injection of AAV-Dre into Ai66(RCFL-tdT) mice gave no tdT+ cells (data not shown). (**C**) Injection of the Cre/Flp double reporter AAV, phSyn1-FSF-FLEX-ChR2(H134R)-EYFP-WPRE-bGHpA (left image) or pCAG-FSF-FLEX-EGFP-WPRE-bGHpA (right image), into the Slc32a1-IRES-Cre;Pvalb-2A-Flpo double driver mouse resulted in labeling of *Slc32a1*+/*Pvalb*+ interneurons. (**D**) Injection of the Cre/Dre double reporter AAV, phSyn1-RSR-FLEX-ChR2(H134R)-EYFP-WPRE-bGHpA, into the Slc32a1-IRES-Cre;Pvalb-2A-Dre double driver mouse resulted in membrane EYFP labeling of *Slc32a1*+/*Pvalb*+ interneurons. (**E**) Injection of the Cre/tTA double reporter AAV, pTRE-FLEX-EGFP-WPRE-bGHpA, into the Emx1-IRES-Cre;Camk2a-tTA double driver mouse resulted in cytoplasmic EGFP labeling of cortical neurons. (**F**) Coinjection of the Cre/Flp/tTA triple reporter AAV, pTRE-FSF-FLEX-EGFP-WPRE-bGHpA, with AAV-Flpo into the Emx1-IRES-Cre;Camk2a-tTA double driver mouse resulted in cytoplasmic EGFP labeling of cortical neurons. (**G**) Coinjection of AAV-Cre and AAV pCAG-FLEX2-tTA2-WPRE-bGHpA into Ai92(TITL-YCX2.60) mouse resulted in robust expression of YCX2.60 in cortical neurons.

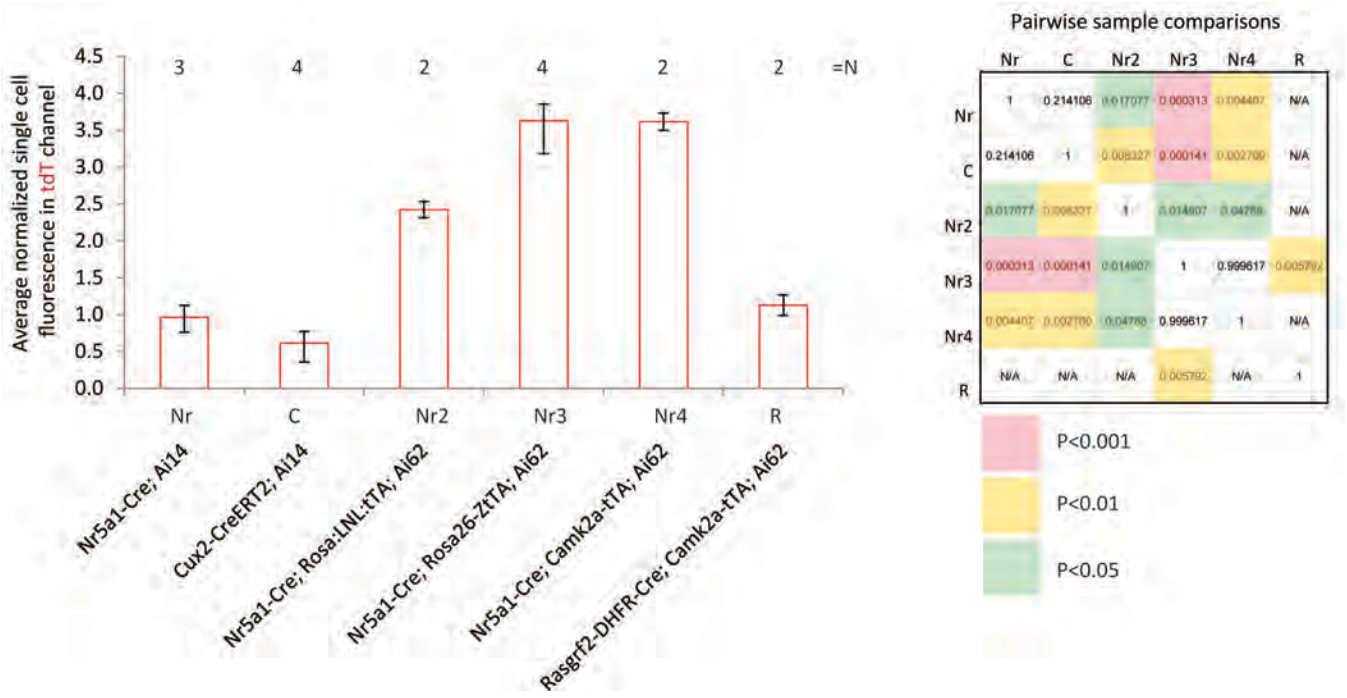

Figure S5. Comparison of average tdTomato reporter expression in individual neurons isolated from different transgenic mice by fluorescence-activated cell sorting (FACS). (Related to **Figure 2**.) Nr5a1-Cre selectively labels cortical layer 4 neurons, Cux2-CreERT2 labels cortical layer 2/3 and 4 neurons, and Rasgrf2-2A-dCre preferentially labels cortical layer 2/3 neurons. Sorting was performed on a BD FACSAriaII SORP with DAPI added to single cell suspension to detect dead cells. The FACS populations analyzed were chosen to include single cells with low DAPI and high tdTomato fluorescence. To correct for the day-to-day differences in laser power, the cellular fluorescence readouts were normalized by signal obtained daily from fluorescent beads (BD Quantibrite PE Beads, BD Biosciences) analyzed using the same laser power settings in the same channel. Subsequently, to simplify comparisons, all average fluorescence values were divided by the average fluorescence for Nr5a1-Cre;Ai14 cells (thereby set at 1). Number of individual replicates (N) for each genotype is shown on top; error bars represent range. Group medians show statistically significant overall variation (Kruskal-Wallis test; chi-squared = 14.7487, df = 5, p = 0.01149). Post-hoc comparisons by Games-Howell test on the left highlight statistically significant pairwise differences (presented as a heatmap of p values; N/A represents pairs in which combined N < 5, and for which the test cannot be applied).

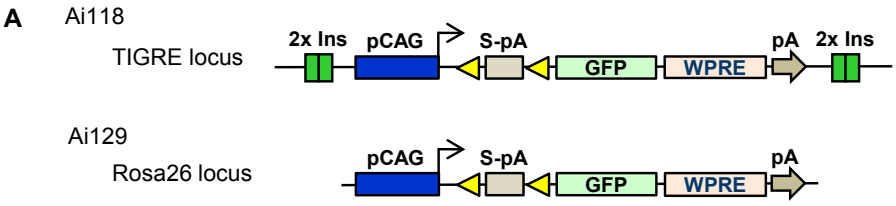

B FACS analysis of clones after transient transfection with CMV-Cre

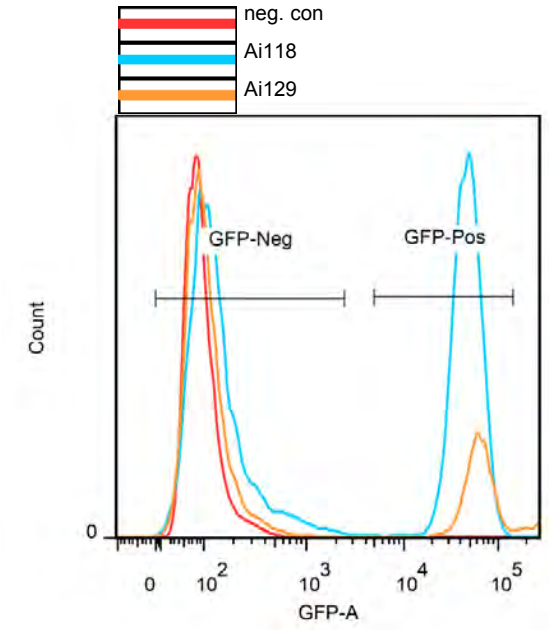

	Mean GFP-	Mean GFP+
Neg. control	91.4	n/a
Ai118,1	173	4.66E4
Ai118,2	154	4.35E4
Ai129,1	112	6.12E4
Ai129,2	165	5.85E4

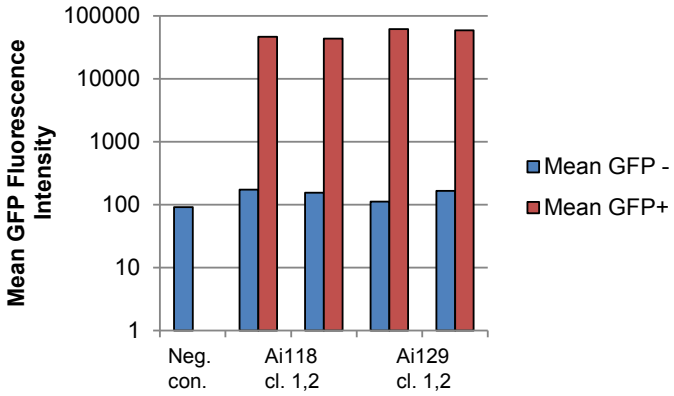

C Sorted GFP+ cells after transient CMV-Cre transfection

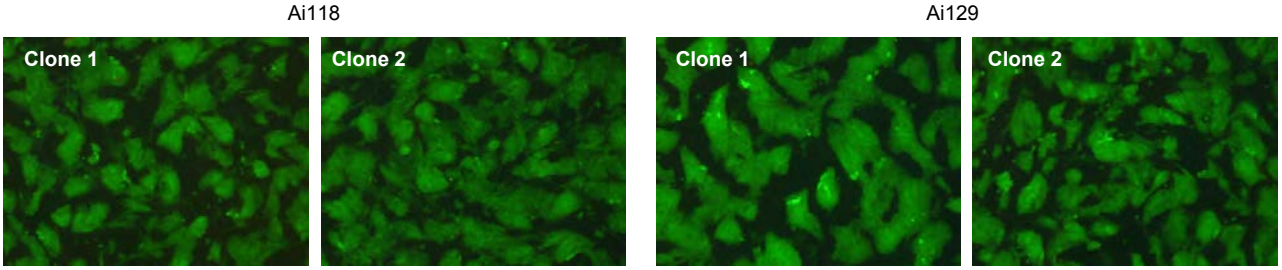

Figure S6. Comparison of EGFP expression in ES clones carrying a pCAG-LSL-EGFP cassette targeted to either the TIGRE locus (Ai118 clones) or the Rosa26 locus (Ai129 clones). (Related to **Figure 2**.) (**A**) Configuration of the two types of targeted ES clones under comparison. (**B**) Transient transfection of 2 independent ES clones from each of Ai118 or Ai129 with a pCMV-Cre plasmid turns on EGFP expression in a portion of the ES cells. FACS analysis of the transfected cells showed two peaks, corresponding to non-Cre-activated EGFP-negative cells and Cre-activated EGFP-positive cells. Comparable GFP fluorescence levels were observed between EGFP+ cells in the Ai118 and Ai129 populations, with Ai129 fluorescence being approximately 30% higher. (**C**) Sorted EGFP+ cells were re-plated and grown in dishes, and they exhibited comparable levels of EGFP fluorescence under the microscope.

Figure S7

A

Emx1-IRES-Cre;Ai35, P147, n=2

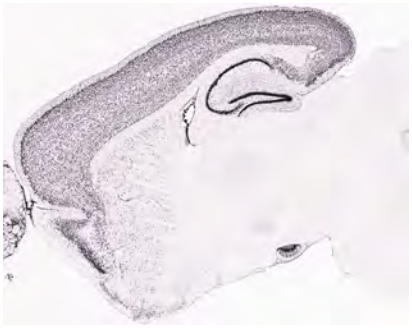

Emx1-IRES-Cre;Ai57(RCL-Jaws), P122, n=2

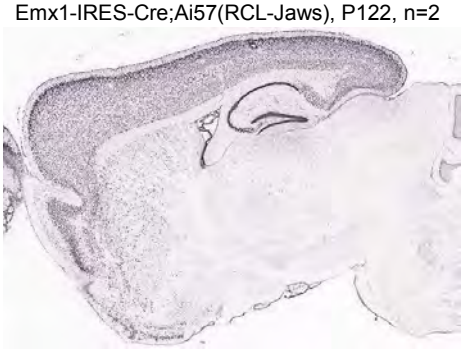

Emx1-IRES-Cre;Camk2a-tTA;Ai79(TITL-Jaws), P330, n=3

Emx1-IRES-Cre;Camk2a-tTA;Ai62(TITL-tdT), P57, n=2

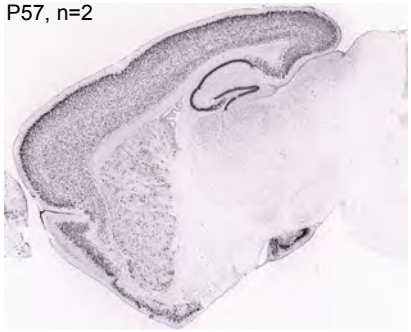

Emx1-IRES-Cre;Ai95(RCL-GCaMP6f), P147, n=1

Emx1-IRES-Cre;Camk2a-tTA;Ai93(TITL-GCaMP6f), P112, n=2

Emx1-IRES-Cre;Ai87(RCL-iGluSnFR), P57, n=1

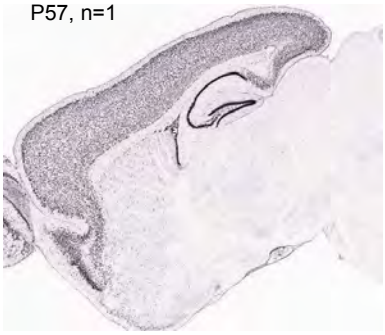

Emx1-IRES-Cre;Camk2a-tTA;Ai85(TITL-iGluSnFR), P56 & P185, n=2

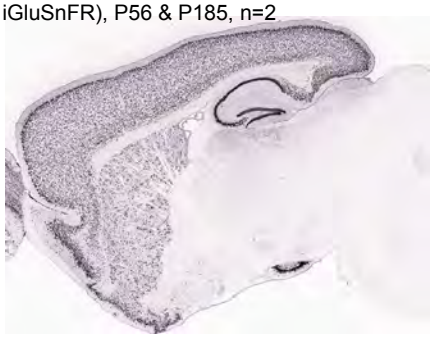

Emx1-IRES-Cre;ROSA26-ZtTA;Ai78(TITL-VSFPB), P76, n=2

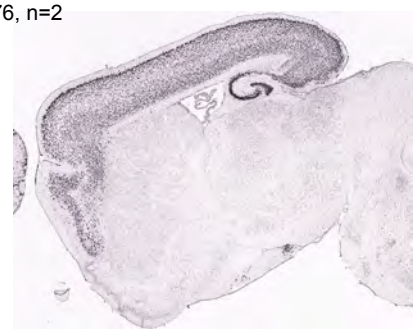

B

Rasgrf2-2A-dCre;Ai14, P56, n=2

Rasgrf2-2A-dCre;Camk2a-tTA; Ai78(TITL-VSFPB), P167, n=1

C

Gad2-IRES-Cre;Ai14, P56, n=5

Gad2-IRES-Cre;ROSA26-ZtTA; Ai92(TITL-YCX2.60), P102, n=2

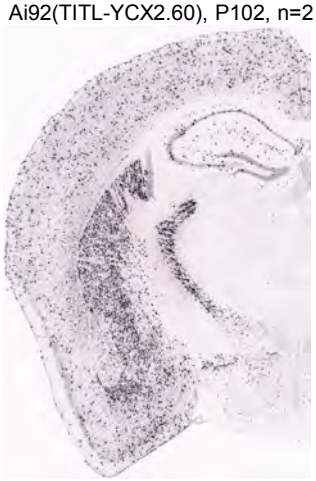

D

Chat-IRES-Cre;ROSA26-ZtTA;Ai93(TITL-GCaMP6f), P95, n=2

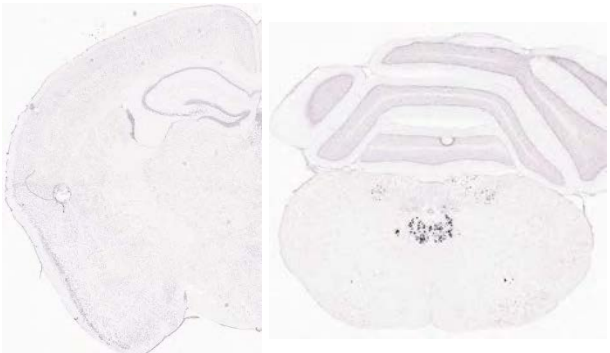

E

Snap25-2A-GCaMP6s, P185, n=4

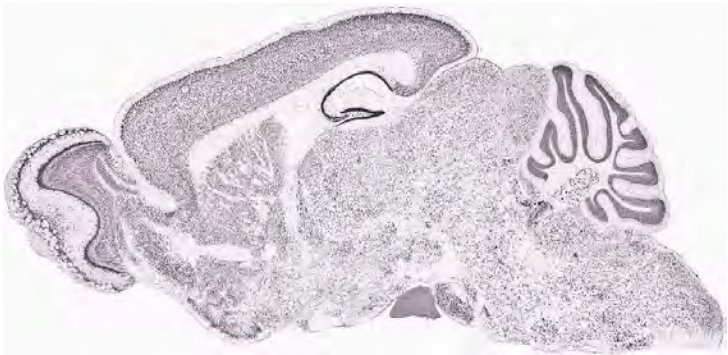

Figure S7. Reporter gene expression patterns in multiple transgenic lines by *in situ* hybridization (ISH). (Related to **Figure 4**.) Number of mice used for ISH for each line and their representative age are shown. EYFP riboprobe was used in all cases except for Ai14 and Ai62 containing specimens in which tdTomato riboprobe was used. Note that expression levels can't be compared reliably between different mice due to the saturation of ISH signals in all three expression systems: Rosa-CAG, TIGRE-TRE and Snap25. (**A**) ISH comparison of various Rosa26 and TIGRE lines under the control of Emx1-IRES-Cre alone, or in combination with Camk2a-tTA or ROSA26-ZtTA. All mice exhibited widespread and high-density expression in cortex, and there was no significant difference in number of expressed cells between different lines or across ages. There is variability in number of expressed cells in striatum. (**B**) ISH comparison between Rosa26 and TIGRE lines under the control of Rasgrf2-2A-dCre alone or in combination with Camk2a-tTA. (**C**) ISH comparison between Rosa26 and TIGRE lines under the control of Gad2-IRES-Cre alone or in combination with ROSA26-ZtTA. In the Gad2-IRES-Cre;ROSA26-ZtTA;Ai92(TITL-YCX2.60) mice, the numbers of expressed cells were moderately reduced in cortex, but substantially reduced in selected subcortical regions. (**D**) In Chat-IRES-Cre;ROSA26-ZtTA;Ai93(TITL-GCaMP6f) mice, there was no detectable reporter gene expression in basal forebrain cholinergic neurons (left panel), although reporter gene was expressed in brainstem cholinergic neurons (right panel). (**E**) Widespread transgene expression throughout the brain in Snap25-2A-GCaMP6s mice.

Figure S8

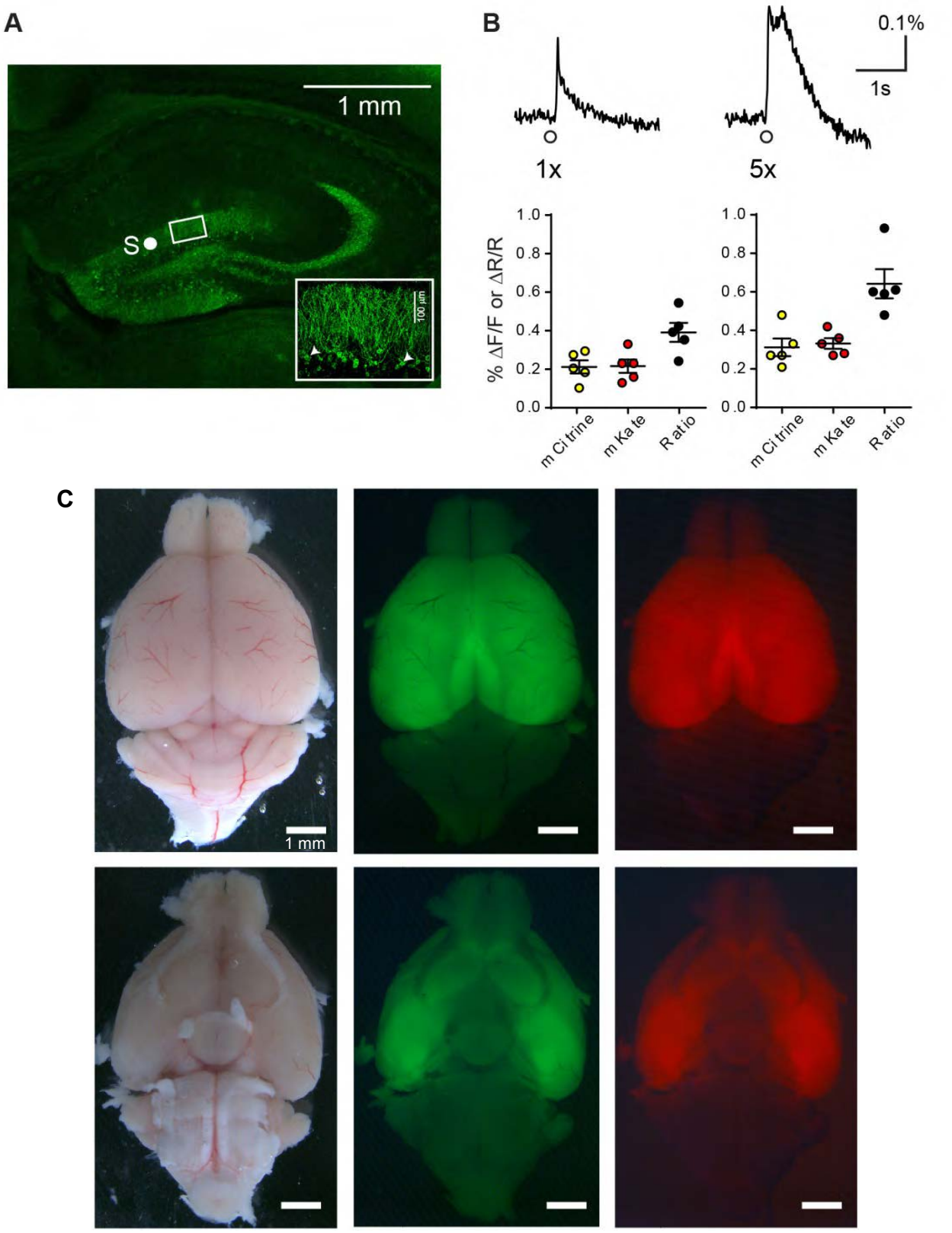
A
1 mm
S
100 µm
B
0.1%
1s
1x
5x
% ΔF/F or ΔR/R
1.0
0.8
0.6
0.4
0.2
0.0
mCitrine
mKate
Ratio
C
1 mm

Figure S8. Functional reporting of population responses from the hippocampus in Rasgrf2-2A-dCre; Camk2a-tTA;Ai78(TITL-VSFPB) mice. (Related to **Figure 5**.) (**A**) Expression of VSFP-Butterfly 1.2 (green) in the dentate gyrus, consistent with expression in granule cells (GCs), inset, examples denoted by arrowheads. (**B**) In 300-µm coronal slices containing the hippocampus, perforant path stimulation (20V at point S, in A) evoked VSFP responses from GC dendrites (rectangular region of interest in A) coincident with field EPSPs (not shown). Repetitive 5x stimulation (100 Hz) evoked larger and longer responses. Traces in upper panels from a single slice, and black symbols in lower panels, are ratios (% ΔR/R) of decreased mCitrine fluorescence (% -ΔF/F, yellow symbols) and increased mKate2 fluorescence (% ΔF/F, red symbols), for 5 recordings from five 2-3 months old mice. Traces are an average of 3 sweeps. Scale bar is 0.1% change in ratio and 1 second, sampling at 100Hz. (**C**) A freshly dissected mouse brain showing the evenness of mCitrine (green) and mKate2 (red) fluorescence of VSFP-Butterfly 1.2 throughout the cortex.

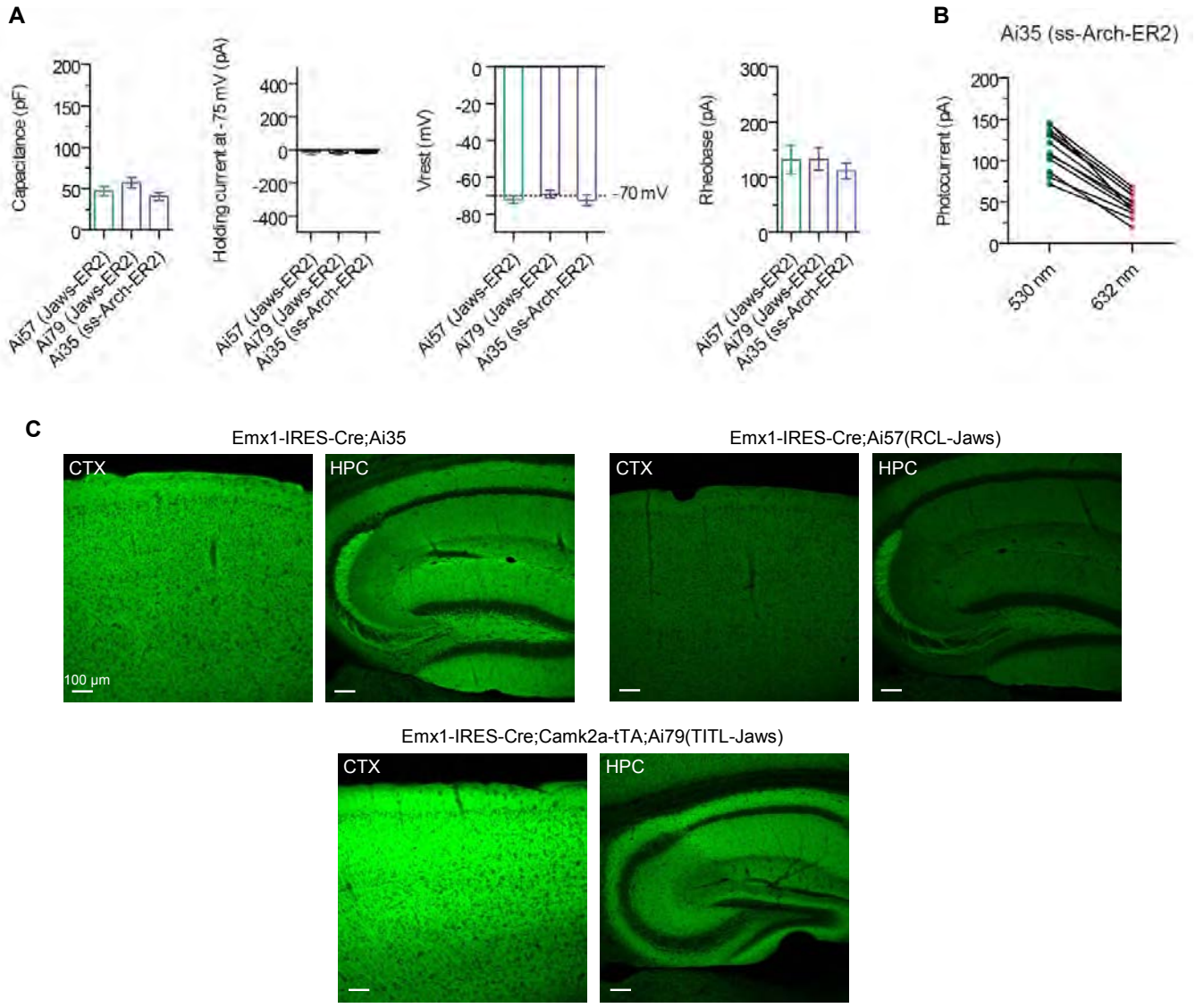

Figure S9. Comparison of expression levels and membrane properties for Emx1-IRES-Cre;Ai57(RCL-Jaws) mice (simplified as Ai57), Emx1-IRES-Cre;Camk2a-tTA;Ai79(TITL-Jaws) mice (simplified as Ai79), and Emx1-IRES-Cre;Ai35 mice (simplified as Ai35). (Related to **Figure 8**.) (**A**) Normal membrane electrophysiological properties in Jaws-expressing neurons in brain slices from Ai57, Ai79 and Ai35 mice. All values represent mean ± SEM. (**B**) Comparison of red or green light (632 or 530 nm; 5 mW/mm^2) induced photocurrents in slices from Ai35 mice. (**C**) Compared to Rosa-CAG based reporter Ai35 which expresses Arch-GFP-ER2, the Rosa-CAG based reporter Ai57 shows weaker fluorescence for Jaws-GFP-ER2, whereas the TIGRE based reporter Ai79 (when combined with Camk2a-tTA) shows stronger fluorescence for Jaws-GFP-ER2. Confocal images were collected at the same time under the same conditions.

Table S1. Transgenic mouse lines used in this study.

Drivers	Originating Lab	Description	Repository Stock #	Official Strain Name
Camk2a-tTA	Mark Mayford	Random insertion: pCamk2a-tTA	JAX 007004	B6.Cg-Tg(Camk2a-tTA)1Mmay/DboJ
Chat-IRES-Cre	Brad Lowell	Knock-into 3' UTR: IRES-Cre	JAX 006410	B6;129S6-Chattm2(cre)Lowl/J
Cux2-CreERT2	Ulrich Mueller	Knock-into ATG: CreERT2	MMRRC 032779	B6(Cg)-Cux2tm3.1(cre/ERT2)Mull/Mmmh
Emx1-IRES-Cre	Kevin Jones	Knock-into 3' UTR: IRES-Cre	JAX 005628	B6.129S2-Emx1tm1(cre)Krj/J
Gad2-IRES-Cre	Z. Josh Huang	Knock-into 3' UTR: IRES-Cre	JAX 010802	STOCK Gad2tm2(cre)Zjh/J
Nr4a2-SA-IRES-Dre	Andras Nagy	Knock-into intron: SA-IRES-Dre		
Nr5a1-Cre	Brad Lowell	Random insertion pNr5a1-Cre	JAX 006364	FVB-Tg(Nr5a1-cre)2Lowl/J
Nxph4-2A-CreERT2	AIBS[a]	Knock-into 3' UTR: T2A-CreERT2	JAX 022861	B6.Cg-Nxph4tm1.1(cre/ERT2)Hze/J
Pvalb-2A-Cre	AIBS	Knock-into 3' UTR: T2A-Cre	JAX 012358	B6.Cg-Pvalbtm1.1(cre)Aibs/J
Pvalb-2A-Dre	AIBS	Knock-into 3' UTR: T2A-DreO	JAX 021190	B6.Cg-Pvalbtm3.1(dreo)Hze/J
Pvalb-2A-Flpo	AIBS	Knock-into 3' UTR: T2A-Flpo	JAX 022730	B6.Cg-Pvalbtm4.1(FLPo)Hze/J
Rasgrf2-2A-dCre	AIBS	Knock-into 3' UTR: T2A-DHFR-Cre	JAX 022864	B6;129S-Rasgrf2tm1(cre/folA)Hze/J
ROSA26-PhiC31	Philippe Soriano	Knock-into intron: SA-PhiC31o-pA-PGKneopA	JAX 007743	B6.129S4-Gt(ROSA)26Sortm3(phiC31*)Sor/J
ROSA:LNL:tTA	Raymond Roos	Knock-in 3' to promoter: loxP-Neo-Stop-loxP-mtTA	JAX 011008	B6.129P2(Cg)-Gt(ROSA)26Sortm1(tTA)Roos/J
ROSA26-ZtTA	Liqun Luo	Knock-into intron: pCA-loxP-β-geo-Stop-loxP-tTA	JAX 012266	STOCK Gt(ROSA)26Sortm5(ACTB-tTA)Luo/J
Scnn1a-Tg3-Cre	AIBS	Random insertion of BAC transgenic at ATG: Cre	JAX 009613	B6;C3-Tg(Scnn1a-cre)3Aibs/J
Slc32a1-IRES-Cre	Brad Lowell	Knock-into 3' UTR: IRES-Cre	JAX 016962	STOCK Slc32a1tm2(cre)Lowl/J
Trib2-2A-CreERT2	AIBS	Knock-into exon 2: F2A-CreERT2	JAX 022865	B6.Cg-Trib2tm1.1(cre/ERT2)Hze/J

Reporters	Genomic Target	Reporter Design	Repository Stock #	Official Strain Name
Ai14	Rosa26	pCAG-LSL-tdTomato-WPRE-bGHpA	JAX 007914	B6.Cg-Gt(ROSA)26Sortm14(CAG-tdTomato)Hze/J
Ai35	Rosa26	pCAG-LSL-ss-Arch-GFP-ER2-WPRE-bGHpA	JAX 012735	B6;129S-Gt(ROSA)26Sortm35.1(CAG-aop3/GFP)Hze/J
Ai62(TITL-tdT)	TIGRE	pTRE-LSL-tdTomato-WPRE-bGHpA	JAX 022731	B6.Cg-Igs7tm62.1(tetO-tdTomato)Hze/J
Ai65(RCFL-tdT)	Rosa26	pCAG-FSF-LSL-tdTomato-WPRE-bGHpA	JAX 021875	B6;129S-Gt(ROSA)26Sortm65.1(CAG-tdTomato)Hze/J
Ai66(RCRL-tdT)	Rosa26	pCAG-RSR-LSL-tdTomato-WPRE-bGHpA	JAX 021876	B6;129S-Gt(ROSA)26Sortm66.1(CAG-tdTomato)Hze/J
Ai57(RCFL-Jaws)	Rosa26	pCAG-FSF-LSL-Jaws-GFP-ER2-WPRE-bGHpA		
Ai72(RCL-VSFPB)	Rosa26	pCAG-LSL-VSFP-Butterfly1.2-WPRE-bGHpA		
Ai78(TITL-VSFPB)	TIGRE	pTRE-LSL-VSFP-Butterfly1.2-WPRE-bGHpA	JAX 023528	B6;129S-Igs7tm78.1(tetO-VSFPB1.2)Hze/J
Ai79(TITL-Jaws)	TIGRE	pTRE-LSL-Jaws-GFP-ER2-WPRE-bGHpA	JAX 023529	B6;129S-Igs7tm79.1(tetO-hop/EGFP)Hze/J
Ai82(TITL-GFP)	TIGRE	pTRE-LSL-EGFP-WPRE-bGHpA	JAX 023532	B6;129S-Igs7tm82.1(tetO-EGFP)Hze/J
Ai85(TITL-iGluSnFR)	TIGRE	pTRE-LSL-iGluSnFR-WPRE-bGHpA		
Ai87(RCL-iGluSnFR)	Rosa26	pCAG-LSL-iGluSnFR-WPRE-bGHpA		
Ai92(TITL-YCX2.60)	TIGRE	pTRE-LSL-YCX2.60-WPRE-bGHpA		
Ai93(TITL-GCaMP6f)	TIGRE	pTRE-LSL-GCaMP6f-WPRE-bGHpA	JAX 024103	B6;129S-Igs7tm93.1(tetO-GCaMP6f)Hze/J
Ai94(TITL-GCaMP6s)	TIGRE	pTRE-LSL-GCaMP6s-WPRE-bGHpA	JAX 024104	B6.Cg-Igs7tm94.1(tetO-GCaMP6s)Hze/J
Ai95(RCL-GCaMP6f)	Rosa26	pCAG-LSL-GCaMP6f-WPRE-bGHpA	JAX 024105	B6;129S-Gt(ROSA)26Sortm95.1(CAG-GCaMP6f)Hze/J
Ai96(RCL-GCaMP6s)	Rosa26	pCAG-LSL-GCaMP6s-WPRE-bGHpA	JAX 024106	B6;129S-Gt(ROSA)26Sortm96(CAG-GCaMP6s)Hze/J
Snap25-LSL-2A-GFP	Snap25	Knock-into exon 8: loxP-Stop-loxP-F2A-EGFP	JAX 021879	B6.Cg-Snap25tm1.1Hze/J
Snap25-2A-GCaMP6s	Snap25	Knock-into exon 8: T2A-GCaMP6s	JAX 025111	B6;129S-Snap25tm3.1(GCaMP6s)Hze/J

[a]AIBS: Allen Institute for Brain Science.

Table S2. Other results.

Other tTA Driver Lines[a]	Genomic Target	Testing Results
Pvalb-2A-tTA2	Knock-into 3' UTR: T2A-tTA2	Pvalb-2A-tTA2 mice showed good tTA-induced reporter expression in the first generation of mice, by injection of AAV-pTRE-ChR2-EYFP into the cortex (no TRE promoter driven reporter line was used at the time). But a few generations later, we found that such expression was largely gone throughout the brain and only expression in some cerebellar Purkinje cells was left. ISH using tTA2 riboprobe in the Pvalb-2A-tTA2 mice still showed expected expression pattern of tTA2 mRNA throughout the brain, but there was no induction of reporter gene. AAV-pTRE-ChR2-EYFP injection into the cortex also resulted in no induction.
Sst-tTA2	Knock-into ATG start site: tTA2	Neither tTA2 expression nor induction was observed.
Rorb-IRES-tTA2	Knock-into 3' UTR: IRES2-tTA2	No induction was observed.
Rorb-2A-tTA2	Knock-into 3' UTR: T2A-tTA2	The mouse (F1 generation so far) had beautiful layer 4 specific reporter induction.
Slc32a1-IRES-tTA2	Knock-into 3' UTR: IRES2-tTA2	The mouse (F1 generation so far) had low-level reporter activation in some but not all interneurons.

Other Recombinase Driver Lines[b]	Genomic Target	Testing Results
Pvalb-IRES-B3	Knock-into 3' UTR: IRES2-mammalianized B3	No recombination in our Rosa26 double reporter allele bearing recognition sites for B3 and Cre.
Pvalb-IRES-KD	Knock-into 3' UTR: IRES2-mammalianized KD	No recombination in our Rosa26 double reporter allele bearing recognition sites for KD and Cre.

Gal4 Driver Lines[c]	Genomic Target	Testing Results
Thy1-Gal4DBD	Random insertion: Thy1.2 promoter driven Gal4 DNA binding domain	When crossed together with Thy1-VP16AD, the reconstituted Gal4 induced strong expression of GFP from an AAV-based UAS-GFP reporter. However, these double transgenic mice exhibited high mortality rate.
Thy1-mGal4DBD	Random insertion: Thy1.2 promoter driven mammalianized Gal4DBD	When crossed together with Thy1-VP16AD, the reconstituted Gal4 induced strong expression of GFP from an AAV-based UAS-GFP reporter. However, these double transgenic mice exhibited high mortality rate.
Thy1-VP16AD	Random insertion: Thy1.2 promoter driven VP16 activation domain	See above.
Pvalb-2A-Gal4	Knock-into 3' UTR: T2A-Gal4	To examine Gal4 expression at an intermediate expression level, we generated Pvalb-2A-Gal4 knock-in mice. The germline transmitted mice again exhibited high mortality rate at ~3-4 postnatal weeks. These results indicate that the Gal4 gene may be toxic in the adult mouse brain. Thus, further testing of this approach was terminated.

[a]In an effort to expand the repertoire of cell type specific tTA driver lines, we generated and tested 5 knock-in tTA lines using the optimized tTA2 version (Urlinger et al., 2000). The testing results are shown here.

[b]We tested the intersection between Cre and two other recombinases, KD and B3, with negative outcomes, although KD and B3 work well to regulate expression in *Drosophila* and have been reported as having activity in mammalian cells (Nern et al., 2011).

[c]The yeast Gal4/UAS system was first introduced in mice as a binary expression system (Ornitz et al., 1991). It has been widely used in *Drosophila* for cell-specific gene expression (Jenett et al., 2012), and a split-Gal4 system has been developed as an intersectional strategy in *Drosophila* (Luan et al., 2006). However, the literature reports limited use of Gal4 in the mouse brain, and then only during neural development in juvenile mice (Hu et al., 2004; Rowitch et al., 1999). As part of our evaluation of various intersectional approaches, we generated Thy1.2 promoter (Caroni, 1997) driven transgenic lines expressing split-Gal4 components (i.e. Gal4-DBD, AD-VP16) (Luan et al., 2006), and knock-in line expressing Gal4 in the *Pvalb* locus. The testing results are shown here.

Movie S1. Two-Photon imaging at 120 μm below the pia in visual cortex of an Emx1-IRES-Cre;Ai95(RCL-GCaMP6f) mouse, matching dataset used in **Figure 7D**. (Related to **Figure 7**.) Visual stimuli were presented to the mouse during the data acquisition period.

Movie S2. Two-Photon imaging at 300 μm below the pia in visual cortex of an Emx1-IRES-Cre;Ai95(RCL-GCaMP6f) mouse, matching dataset used in **Figure 7D**. (Related to **Figure 7**.) Visual stimuli were presented to the mouse during the data acquisition period.

Movie S3. Two-Photon imaging at 120 μm below the pia in visual cortex of an Emx1-IRES-Cre;Camk2a-tTA;Ai93(TITL-GCaMP6f) mouse, matching dataset used in **Figure 7E**. (Related to **Figure 7**.) Visual stimuli were presented to the mouse during the data acquisition period.

Movie S4. Two-Photon imaging at 300 μm below the pia in visual cortex of an Emx1-IRES-Cre;Camk2a-tTA;Ai93(TITL-GCaMP6f) mouse, matching dataset used in **Figure 7E**. (Related to **Figure 7**.) Visual stimuli were presented to the mouse during the data acquisition period.

SUPPLEMENTAL EXPERIMENTAL PROCEDURES

Transgenic mice generation

Targeting constructs were generated using a combination of molecular cloning, gene synthesis (GenScript, Piscataway, US) and Red/ET recombineering (Gene Bridges, Heidelberg, DE). Coding sequences for the fluorescent proteins and optogenetic tools included in the Ai reporter lines listed in **Table 1** were cloned between the LSL cassette and the WPRE element in the targeting backbones described below, either directly from acquired plasmids or after gene synthesis based on published information. The 129S6B6F1 ES cell line, G4, was used to generate all transgenic mice by homologous recombination and, in many cases, subsequent Flp- recombinase-mediated cassette exchange (RMCE). Correct clones were used in blastocyst injections to obtain germline transmission. Resulting mice were crossed to the Rosa26-PhiC31 mice (JAX Stock # 007743) to delete the pPGK-neo or pPGK-hygro selection marker cassette, and then backcrossed to C57BL/6J mice and maintained in C57BL/6J congenic background.

Rosa26-pCAG-LSL-WPRE-bGHpA (RCL) vectors: Vector backbone has been previously described (Madisen et al., 2010) and contains a loxP – stop codons – 3x SV40 polyA – loxP cassette.

Rosa26-pCAG-FSF-LSL-WPRE-bGHpA (RCFL) and Rosa26-RSR-LSL-WPRE-bGHpA (RCRL) vectors: The original Rosa26 targeting vector above was modified to include an additional stop cassette between the CAG promoter and the loxP – stop codons – 3x SV40 polyA – loxP unit. The additional stop cassettes contained: FRT (or Rox) – an 8 amino acid open reading frame – stop codons – a synthetic polyA – hGH polyA – TK polyA – FRT (or Rox). Note that the new stop cassette in FSF and RSR is different from the previously created stop cassette in LSL, to reduce the sequence repetitiveness in the new targeting vectors.

TIGRE vectors: As shown in **Figure S1B**, ES clones carrying TIGRE reporters were generated by a recombinase-mediated cassette exchange (RMCE) strategy into an ES clone that had been first targeted with a Flp/FRT-based docking site. In our first step to generate this ES clone with a docking site inserted into the TIGRE locus, the original targeting vector contained: 5' and 3'homology arms (base pairs 21539059-21545314 and 21545315-21549209, respectively, of ref_NC 000075.6 on mouse chromosome 9) flanking the following cassette: FRT3 (F3) – AttB – pPGK – neomycin-resistant gene – PGK polyA – FRT5 (F5) – mRNA splice acceptor – domain 2 from the hygromycin-resistant gene – SV40 polyA – AttP. Southern blot analysis was done on neo resistant ES clones to confirm correct construct integration. Several targeted clones were injected into blastocysts, and those that gave rise to high-percentage chimeras were chosen for expansion and use in the RMCE transfections.

Replacement vectors used for RMCE into the TIGRE docking site: The replacement vectors were in the following configuration (**Fig. S1B**): F3 – 2 copies of the 1.2-kb chicken β-globin HS4 insulator fragment – pTRE-Tight – loxP – an 8 amino acid open reading frame – stop codons – a synthetic polyA – hGH polyA – PGK polyA – loxP – Transgene – WPRE – bGH polyA – 2 copies of the 1.2-kb chicken β-globin HS4 insulator fragment – AttB – pPGK – domain 1 from the hygromycin-resistant gene – mRNA splice donor – F5. The TRE promoter used here was from Clontech's pTRE-Tight vector, which contains a modified Tet response element (TREmod) that consists of seven direct repeats of a 36-bp sequence containing the 19-bp tet operator sequence (tetO); the TREmod is just upstream of the minimal CMV promoter. Supercoiled replacement vectors were co-transfected with a pCAG-Flpe plasmid into the above TIGRE docking clones and selected with hygromycin. Resistant colonies were screened for correct 5' and 3' junctions and for the lack of the original docking site sequence. The general configuration of the replacement vector was modified to generate the Ai118 line (**Fig. S6**), in which the TRE-pCMVmin promoter was replaced by the CAG promoter present in all Rosa26 reporter constructs.

Pvalb-targeted vectors: The *Pvalb* locus was originally targeted with homologous recombination to insert T2A-Cre at the endogenous stop codon (Madisen et al., 2010), using a targeting vector containing the following components (**Fig. S1A**): 5' arm – F3 – last ~250bp of intron 3 – exon 4 up to the endogenous stop codon – T2A-Cre – stop codon – Pvalb 3' UTR – AttB – pPGK – neomycin-resistant gene – PGKpA – F5 – mRNA splice acceptor – domain 2 from the hygromycin-resistant gene – SV40 polyA – AttP – 3' arm. Correctly targeted neomycin resistant clones were identified by PCR, and then confirmed by Southern blot. One clone that gave high percentage chimeras following blastocyst injection was used in subsequent RMCE experiments. Replacement vectors included: F3 – last ~250bp of intron 3 – exon 4 up to the endogenous stop codon – T2A-Transgene (Flpe/Flpo/Dre) – stop codon – Pvalb 3' UTR – AttB – pPGK – domain 1 from the hygromycin-

resistant gene – mRNA splice donor – F5. Following co-transfection with a pCAG-Flpe plasmid, hygromycin resistant colonies were screened for correct 5' and 3' junctions and for lack of the original vector sequence.
Snap25-targeted vectors: The *Snap25* locus was targeted with homologous recombination to insert LSL-F2A-GFP at the endogenous stop codon, using a targeting vector containing the following components: 5' arm – F3 – last ~300bp of intron 7 – exon 8 up to the endogenous stop codon – loxP – stop codons – PGK polyA – loxP – F2A – EGFP – WPRE – bGH polyA – AttB – pPGK – neomycin-resistant gene – PGKpA – F5 – mRNA splice acceptor – domain 2 from the hygromycin-resistant gene – SV40 polyA – AttP – 3' arm. Correctly targeted neomycin resistant clones were identified by PCR, and then confirmed by Southern blot. One clone that gave high percentage chimeras following blastocyst injection was used in a RMCE transfection to switch the LSL-F2A-GFP expression unit for a T2A-GCaMP6s expression unit. The replacement vector included: F3 – last ~250bp of intron 7 – exon 8 up to the endogenous stop codon – T2A-GCaMP6s – WPRE – bGH polyA – AttB – pPGK – domain 1 from the hygromycin-resistant gene – mRNA splice donor – F5. Following co-transfection with a pCAG-Flpe plasmid, hygromycin resistant colonies were screened for correct 5' and 3' junctions and for lack of the original vector sequence.
Nr4a2-SA-IRES-Dre vector: Targeted mice were generated in collaboration with the NorCOMM high throughput gene targeting project (http://www.norcomm.org/index.htm). The *Nr4a2* locus was targeted with a vector that results in deletion of the protein encoding sequence and replacement with an F3 – mRNA splice acceptor – IRES-Dre – FRT cassette. A mammalian codon-optimized Dre was used here.
Rasgrf2-targeted vector: The *Rasgrf2* locus was targeted with homologous recombination to insert T2A-dCre at the endogenous stop codon, using a targeting vector containing the following components: 5' arm – F3 – last ~300bp of intron 33 – exon 34 up to the endogenous stop codon – T2A-dCre – bGH polyA – AttB – pPGK – neomycin-resistant gene – PGKpA – F5 – mRNA splice acceptor – domain 2 from the hygromycin-resistant gene – SV40 polyA – AttP – 3' arm. The dCre fusion gene (also called destabilized Cre, hDHFR/Cre or ecDHFRR12Y/Y100I/Cre) is Cre recombinase fused at its N-terminus to the first 159 amino acids of the *E. coli* K-12 dihydrofolate reductase gene, harboring G67S and R12Y/Y100I destabilizing domain mutations (Sando et al., 2013). Activity of dCre recombinase is low in the absence of trimethoprim (TMP), and full Cre activity was induced in these mice by an intraperitoneal (IP) injection of TMP at 0.25 mg/g body weight per day for 3 days. Since TMP has low solubility in aqueous solution, 10x stock solution in 100% DMSO needs to be quickly diluted with 0.9% saline and immediately (within 1 min) injected into mice. Alternatively, TMP can be diluted from a 10x stock in 100% DMSO with a 2% methylcellulose solution and administered via oral gavage (PO) at 0.3 mg/g body weight per day for 3 days. Mice can be used for experiments starting at 1-2 weeks after dosing.

Transgenic mice expression characterization
Driver and reporter lines were crossed together according to specific schemes. Expression of the reporter genes was assessed by native fluorescence (without antibody staining) on perfused, microtomed sections or by *in situ* hybridization (ISH) on fresh-frozen sections.
For analysis of native fluorescence, animals were perfused with 4% paraformaldehyde (PFA) in 0.1 M PB. Brains were fixed for an additional 18 hr at 4°C, then cryoprotected in 10% sucrose in PBS at 4°C overnight. Brains were sectioned to 100 µm using a Leica SM2000R sliding microtome and sections were mounted onto slides. The sections were examined by epifluorescence microscopy without antibody staining. For confocal imaging, sections were imaged using an Olympus FV1000 confocal system with 10x or 20x objectives. To keep imaging conditions constant for comparison purposes, laser power was always set at 10%, whereas PMT gain was adjusted to stay within proper dynamic range but kept constant within each group of brains being compared and the value was reported for each confocal image shown in this paper.
For FACS sorting and quantification of fluorescence level, single cell suspensions of live cells were analyzed for mean fluorescence intensity on a BD FACSAria II SORP instrument using settings optimized for side and forward scatter. Wild-type cells were used as a negative control, and doublets, debris and DAPI+ dead cells were gated out. Graphics were done with FloJo.
For ISH, we used the Allen Institute–established pipelines for tissue processing, riboprobe hybridization, image acquisition and data processing (Lein et al., 2007; Madisen et al., 2010). Riboprobes used for expression profiling ISH were designed against Cre, tdTomato and EYFP/EGFP. All transgenic mice ISH data can be found at the Transgenic Characterization database (http://connectivity.brain-map.org/transgenic/search/basic) (Harris et al., 2014).

Hippocampal slice recording of VSFP activities

We prepared acute coronal slices (300 μm thick) containing cortex and hippocampus (vibratome VTS1000S, Leica). The mice (2-3 months old) were sedated by exposure to CO_2 gas, decapitated, the brain immediately removed and submerged in ice-cold cutting solution (in mM: 87 NaCl, 75 sucrose, 2.5 KCl, 6 $MgCl_2$, 0.5 $CaCl_2$, 25 Glucose, 25 $NaHCO_3$, 1.25 NaH_2PO_4) saturated with 95% O_2 and 5% CO_2. The slices were transferred to artificial cerebrospinal fluid (ACSF) containing (in mM) 126 NaCl, 3 KCl, 1 NaH_2PO_4, 2 $MgSO_4$, 2 $CaCl_2$, 25 $NaHCO_3$, 15 glucose, saturated with 95% O_2 and 5% CO_2, and maintained initially at 35ºC for 30 min and then at room temperature for at least another 30 min before recording.

Slices were transferred to the recording chamber of an upright microscope (Eclipse FN1, Nikon). The dentate gyrus was imaged with a 16× water immersion objective (Nikon) using fluorescence excitation (mCitrine, 483/32-25, Semrock FF01) from a halogen lamp (Moritex Corporation, Japan) and emission (542/27-25 for mCitrine, Semrock FF01; and 594R-25 for mKate, Semrock BLP01) collected with a cooled CCD camera (Hamamatsu C-9100), at 118 Hz (4× binning) Simple PCI (Hamamatsu Corporation, Japan). Electrical synaptic stimulation was synchronized with a Master 8 (A.M.P.I., Israel) and used an ACSF-filled glass electrode (approximately 1 MΩ) placed in the middle of the molecular layer approximately 200-400 μm from the recording region of interest (ROI). Fluorescence signals from a single ROI placed in the molecular layer of the dentate gyrus were bleach corrected by subtracting stimulated responses from non-stimulated responses, both averaged 3-5 times, using Excel.

***In vivo* wide-field voltage imaging**

Six mice were imaged repeatedly between the ages of 3 to 9 months. The mice were implanted with a head plate and an 8 mm circular window for imaging through thinned skull, as described elsewhere (Drew et al., 2010). During imaging experiments, the animal was placed on a spherical treadmill, where it was allowed to move freely while its head was held fixed for imaging. To excite the donor fluorophore (mCitrine), we diverted a blue LED light (LEX2-B, Brainvision Inc.) onto the cortex via a dichroic mirror (FF506-Di03, Semrock Inc.). To acquire both fluorophores we used two sCMOS cameras (pco.edge, PCO AG). The first camera recorded the emitted fluorescence from mCitrine, which was reflected by a second dichroic mirror (FF593-Di03, Semrock Inc.), passed through an emission filter (FF01-543/50-25, Semrock Inc.). The second camera recorded the emitted fluorescence from mKate2, passed through the second dichroic mirror and an emission filter (BLP01-594R-25, Semrock Inc.). These cameras were controlled by an external TTL pulse synchronized with the sensory stimulation. The image acquisition rate was 50 Hz, with a nominal spatial resolution of 123 pixels/mm.

Stimuli were trains of visual, somatosensory, or auditory stimuli, delivered to elicit periodic responses in cortex. Stimulus trains were typically presented for 5 s and repeated 20 times for each modality. For retinotopy mapping, 4 different positions and the no-stimulus condition were randomized. For somatosensory and auditory mapping, air puff, sham of air puff, auditory tone, and the no-stimulus conditions were randomized. Visual stimuli were presented via LCD monitors placed 20-30 cm away from the animal. Horizontal or vertical contrast-reversing bars or gratings were presented inside a rectangular window (reversal frequency 2 Hz, spatial frequency 0.03 cycles/deg). These stimuli elicit cortical responses at twice the reversal frequency (4 Hz). To measure preferred azimuth, the rectangular window was 60° high and 20° wide. To measure preferred elevation, it was 15° high and 60° wide. Somatosensory stimuli were trains of air puffs delivered from a spritzer (Pressure system IIe, Toohey Company) towards the whiskers at a pressure of 20 PSI via silicone tube (0.5 mm open tip diameter). Air puffs lasted 20 ms and were repeated at 4 Hz. To control for the effect of the sound, sham air puffs were randomly interleaved and delivered away from the whiskers. Auditory stimuli were trains of tones delivered at 80 dB_{SPL} via a magnetic speaker (Tucker-Davis Technologies) placed 15 cm in front of the animal. Each tone lasted 50 ms, and was repeated at 6 Hz. Tones of different frequencies were randomly interleaved.

To eliminate slow (hemodynamic) components of the optical signals, image sequences were high-pass filtered with a causal Butterworth filter (0.5 Hz corner frequency). The image sequences were then normalized by the data during prestimulus period. The voltage signal was calculated as the ratio of acceptor and donor signals from the two cameras, after aligning them (with Matlab's Image Processing Toolbox) and equalizing fluctuation at the heartbeat frequency (Akemann et al., 2012). We then averaged the images across repeats, and measured the amplitude of the oscillation of each pixel at the response frequency (4 Hz for visual stimuli and air puffs, 6 Hz for tones). We then smoothed the resulting maps with a Gaussian filter (sigma = 97 μm). The map of retinotopy was estimated by fitting the response amplitudes for different stimulus positions (azimuth or elevation) with a

Gaussian function. The width of the Gaussian function (sigma) was estimated as a global parameter across pixels. To obtain the map of tonotopy, the same algorithm was applied to the response amplitudes for different tone frequencies. To calculate signal-to-noise ratio during visual stimulation, we took the responses to a vertical flickering bar presented to the monocular zone. We obtained a map of signal-to-noise ratio (S/N) as the 4 Hz amplitude during the stimulation (averaged over 12 trials), divided by the 4 Hz amplitude during no-stimulation. To estimate S/N for each animal, we picked all the pixels within 0.5 mm from the pixel that showed the highest signal, and averaged the S/N over those pixels.

***In vivo* two-photon calcium imaging in GCaMP6 mice**

Each mouse received surgery for head-plate implantation and a craniotomy for glass window placement over visual cortex starting at age P45. A metal head-plate was cemented to the skull and a 5 mm circular craniotomy was made. Two 5 mm and one 8 mm circular glass cover slips were glued together and fitted into the craniotomy. The 8 mm coverslip rested against the surface of the skull and was cemented in place. Mice were allowed 7 days to recover from surgery and were then habituated to head fixation and the experimental set-up including visual stimuli for 5 to 14 days depending on the temperament of the mouse.

During experiments, the animal was permitted to run on a freely-rotating disc while visual stimuli were presented to the eye contralateral to the imaged region. Visual stimuli and software for tracking motion of the mouse were created in Python. Stimuli consisted of drifting sinusoidal gratings presented at 80% contrast shown in random order for all permutations of 5 spatial frequencies (SF), 5 temporal frequencies (TF), and 8 orientations (0° to 315° in 45° steps). Stimuli were presented 8 times each, full-field, for 3 seconds with a mean luminance inter-stimulus-interval of 2 seconds on an LCD monitor spanning 60° in elevation and 130° in azimuth. The mouse's eye was positioned 22 cm away from the center of the monitor.

Image data were acquired using a custom built two-photon microscope with resonant scanners, and a MaiTai femtosecond laser (Spectra-Physics) at 920 nm through a 16x water-immersion objective lens (Nikon, NA 0.8). Images were collected at approximately 30 Hz with 512 lines per frame. Laser powers (at objective) used were 100 mW (at 120 μm depth) and 130 mW (at 300 μm depth) for Ai95 mice, 90 mW (at 120 μm depth) and 120 mW (at 300 μm depth) for Ai93 mice. Data analysis was performed in Python and Matlab. In summary, data was down-sampled to 4 Hz and motion corrected using cross-correlation between frames. Segmentation was achieved by either using Independent Component Analysis (ICA) followed by automated Region of Interest (ROI) selection or by manually selection of ROIs, and traces were extracted by averaging all pixels in a segment and measuring their fluorescence over time. The background for $\Delta F/F$ calculation was determined using a sliding window to find a local minimum for fluorescence for the duration of the experiment. Tuning was calculated from the averaged response over the full 3 seconds of stimulus presentation.

***In vivo* two-photon calcium imaging in YCX2.60 mice**

Adult mice (>P45) were implanted with a 3-mm cranial window above the barrel field in somatosensory cortex and a head post. YCX2.60 expression was induced by i.p. injection of Trimethoprim (TMP) one week before imaging (dissolved in DMSO and diluted with saline; dosage: 150 μg/g body weight).

Mice were anesthetized with 0.5-0.8% isofluorane and body temperature was maintained at 37ºC with a heating blanket. We identified the barrel column corresponding to the C2 whisker using intrinsic optical imaging. The C2 whisker was stimulated with a piezoelectric element (2º amplitude in the rostrocaudal direction at 10 Hz) and reflectance images were acquired with red light illumination of the cortical surface (630-nm light-emitting diode, LED). Images were collected through a 4x objective with a CCD camera (Toshiba TELI CS3960DCL; 12-bit; 3-pixel binning, 427x347 binned pixels, 8.6 μm pixel size, 10 Hz frame rate). The intrinsic signal of the C2 barrel column was mapped to the blood vessel reference image, which was obtained with green light illumination (546-nm LED).

Two-photon calcium imaging of somatosensory cortex was performed with a custom-built two-photon microscope using galvanometric scanners and a Ti:sapphire laser system (Mai Tai Deep See; Newport Spectra-Physics). Fluorescence images of 128x64 pixels were acquired at 15 Hz through a 16x water-immersion objective lens (Nikon, NA 0.8). YCX2.60 fluorescence excited at 840-nm wavelength with 40 mW laser power after objective was collected in two spectral channels using blue (480/60 nm) and yellow (542/50 nm) emission filters. ROIs of active cells were manually annotated, and fluorescence traces were extracted by subtracting background and averaging all ROI pixels for each channel (CFP and YFP, respectively). The ratio R was calculated as the

ratio of the YFP and the CFP signals. Fluorescence traces were also expressed as relative percentage changes $\Delta R/R = (R-R_0)/R_0$ with the baseline ratio R_0 determined as the bottom 10^{th} percentile of the ratio trace.
For *in vitro* measurements of yellow cameleon properties, 3 days after transfection using Lipofectamine 2000 (Invitrogen), HeLa cells expressing YC2.60 or YCX2.60 were imaged on an inverted microscope (IX73, Olympus) with a dual CCD camera (ORCA-D2, Hamamatsu). A 440DF20 excitation filter, a 455DRLP dichroic mirror and optical block A11400-03 in ORCA-D2 (dichroic mirror 510 nm, 483/32 nm for CFP, 542/27 nm for YFP) were used for dual-emission imaging. The sequence for YCX2.60 has been deposited in the DDBJ/EMBL/GenBank databases (accession number LC025957).

***In vitro* and *in vivo* electrophysiology of optogenetic silencing**
All light powers were measured with a PM200B photodetector (Thorlabs); all *in vivo* light powers were reported as measured at a 200-μm fiber tip with an integrating sphere (S142C, Thorlabs) rather than calculated at a distance away from the fiber (Chuong et al., 2014).
In vivo extracellular recordings were conducted as before (Chuong et al., 2014). Briefly, adult (2-7 months old) mice were implanted with a metal headplate and a circular craniotomy was made over the primary visual cortex. Extracellular recordings were conducted in the cortex of awake, head-fixed mice using 3-10 MΩ saline-filled glass microelectrodes containing silver/silver-chloride electrodes. Signals were amplified with a Multiclamp 700B and digitized with a Digidata 1440B, using pClamp software (Molecular Devices). A recording glass electrode was attached to a 200-μm diameter optical fiber, coupled to a 637 nm laser (Coherent Lasers), such that the fiber tip was 500 ± 50 μm above the tip of the electrode, and guided into the brain with a Sutter manipulator. Light pulses were controlled via Digidata-generated TTL pulses, and data was analyzed using MATLAB and Offline Sorter (Plexon). Light-modulated units were identified by performing a paired t-test between the 5-s illumination period and the baseline firing period of the same time duration immediately before illumination, thresholding at $P < 0.05$. The degree of suppression was calculated for each cell by dividing the mean firing rate during the light stimulus by the mean baseline firing rate during the same time duration before light stimulation onset.
Ex vivo electrophysiology was carried out with 300-μm brain slices. Mice (2-7 months old) were deeply anaesthetized with isoflurane, then transcardially perfused with 40 ml of ice-cold ACSF (in mM: NaCl 87, KCl 2.5, NaH_2PO4 1.3, $MgCl_2$ 7, $NaHCO_3$ 25, sucrose 75, ascorbate 5, $CaCl_2$ 0.5, in ddH_2O; 320-330 mOsm, pH 7.30-7.40, saturated with 95% O_2 / 5% CO_2). The brain was sectioned using a Compresstome (Precisionary Instruments Inc.) and slices were incubated in ACSF (containing in mM: NaCl 124, KCl 2.5, NaH_2PO4 1.25, $MgSO_4$ 1, $NaHCO_3$ 25, sodium pyruvate 3, sodium L-ascorbate 0.5, myo-inositol 3, taurine 0.01, glucose 10, $CaCl_2$ 1.2, in ddH_2O; 299-301 mOsm; pH 7.35-7.45, saturated with 95% O_2 / 5% CO_2) at 32°C for ≥ 90 min before being transferred to the recording chamber for electrophysiology. Once in the recording chamber, slices were continuously perfused at a rate of 2 ml/min with fully oxygenated ACSF at 32°C with added Picrotoxin (100 μM) and kynurenic acid (1 mM) to block GABAergic and glutamatergic synaptic transmission. Neurons were identified under DIC based on pyramidal morphology rather than fluorescence and optical activation with 500-ms light pulses was delivered using 530 or 625 nm LEDs (Thorlabs). The 625 nm LED was additionally filtered with a 632 nm ± 11 nm filter (Semrock). 4–6 MΩ borosilicate glass pipettes (Kings Precision Glass) filled with internal solution (containing (in mM): potassium gluconate 120, KCl 7, EGTA 1, HEPES 10, Mg-ATP 3, Na-GTP 0.4, phosphocreatine 10; 290 mOsm; pH 7.3) were used for whole-cell patch-clamp recording in slice. During recording, membrane capacitance (Cm), series resistance (Rs) and input resistance (Rin) were frequently monitored. Cells with Vrest > −60 mV, Rs > 30 MΩ or Rs/Rin changed over 30% during recording were excluded from final data analysis.

SUPPLEMENTAL REFERENCES

Akemann, W., Mutoh, H., Perron, A., Park, Y.K., Iwamoto, Y., and Knopfel, T. (2012). Imaging neural circuit dynamics with a voltage-sensitive fluorescent protein. J. Neurophysiol. *108*, 2323-2337.
Caroni, P. (1997). Overexpression of growth-associated proteins in the neurons of adult transgenic mice. J Neurosci Methods *71*, 3-9.
Chuong, A.S., Miri, M.L., Busskamp, V., Matthews, G.A., Acker, L.C., Sorensen, A.T., Young, A., Klapoetke, N.C., Henninger, M.A., Kodandaramaiah, S.B.*, et al.* (2014). Noninvasive optical inhibition with a red-shifted microbial rhodopsin. Nat. Neurosci. *17*, 1123-1129.
Drew, P.J., Shih, A.Y., Driscoll, J.D., Knutsen, P.M., Blinder, P., Davalos, D., Akassoglou, K., Tsai, P.S., and Kleinfeld, D. (2010). Chronic optical access through a polished and reinforced thinned skull. Nat. Methods *7*, 981-984.
Harris, J.A., Hirokawa, K.E., Sorensen, S.A., Gu, H., Mills, M., Ng, L.L., Bohn, P., Mortrud, M., Ouellette, B., Kidney, J.*, et al.* (2014). Anatomical characterization of Cre driver mice for neural circuit mapping and manipulation. Front. Neural Circuits *8*, 76.
Hu, Q., Ueno, N., and Behringer, R.R. (2004). Restriction of BMP4 activity domains in the developing neural tube of the mouse embryo. EMBO Rep *5*, 734-739.
Jenett, A., Rubin, G.M., Ngo, T.T., Shepherd, D., Murphy, C., Dionne, H., Pfeiffer, B.D., Cavallaro, A., Hall, D., Jeter, J.*, et al.* (2012). A GAL4-driver line resource for Drosophila neurobiology. Cell Rep *2*, 991-1001.
Lein, E.S., Hawrylycz, M.J., Ao, N., Ayres, M., Bensinger, A., Bernard, A., Boe, A.F., Boguski, M.S., Brockway, K.S., Byrnes, E.J.*, et al.* (2007). Genome-wide atlas of gene expression in the adult mouse brain. Nature *445*, 168-176.
Luan, H., Peabody, N.C., Vinson, C.R., and White, B.H. (2006). Refined spatial manipulation of neuronal function by combinatorial restriction of transgene expression. Neuron *52*, 425-436.
Madisen, L., Zwingman, T.A., Sunkin, S.M., Oh, S.W., Zariwala, H.A., Gu, H., Ng, L.L., Palmiter, R.D., Hawrylycz, M.J., Jones, A.R.*, et al.* (2010). A robust and high-throughput Cre reporting and characterization system for the whole mouse brain. Nat. Neurosci. *13*, 133-140.
Nern, A., Pfeiffer, B.D., Svoboda, K., and Rubin, G.M. (2011). Multiple new site-specific recombinases for use in manipulating animal genomes. Proc. Natl. Acad. Sci. USA *108*, 14198-14203.
Ornitz, D.M., Moreadith, R.W., and Leder, P. (1991). Binary system for regulating transgene expression in mice: targeting int-2 gene expression with yeast GAL4/UAS control elements. Proc. Natl. Acad. Sci. USA *88*, 698-702.
Rowitch, D.H., B, S.J., Lee, S.M., Flax, J.D., Snyder, E.Y., and McMahon, A.P. (1999). Sonic hedgehog regulates proliferation and inhibits differentiation of CNS precursor cells. J. Neurosci. *19*, 8954-8965.
Sando, R., 3rd, Baumgaertel, K., Pieraut, S., Torabi-Rander, N., Wandless, T.J., Mayford, M., and Maximov, A. (2013). Inducible control of gene expression with destabilized Cre. Nat. Methods *10*, 1085-1088.
Urlinger, S., Baron, U., Thellmann, M., Hasan, M.T., Bujard, H., and Hillen, W. (2000). Exploring the sequence space for tetracycline-dependent transcriptional activators: novel mutations yield expanded range and sensitivity. Proc. Natl. Acad. Sci. USA *97*, 7963-7968.